Attosecond pulse metrology Ⓕ

I. Orfanos, I. Makos, I. Liontos ⓘD, E. Skantzakis ⓘD, B. Förg, D. Charalambidis, and P. Tzallas

COLLECTIONS

Ⓕ   This paper was selected as Featured

View Online   Export Citation   CrossMark

ARTICLES YOU MAY BE INTERESTED IN

2D optical materials and the implications for photonics
APL Photonics **4**, 080401 (2019); https://doi.org/10.1063/1.5120030

Hybrid plasmonic waveguide coupling of photons from a single molecule
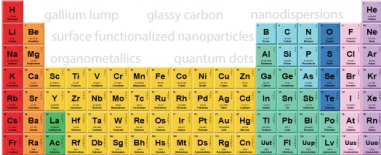APL Photonics **4**, 086101 (2019); https://doi.org/10.1063/1.5110275

Background-free time-resolved coherent Raman spectroscopy (CSRS and CARS):
Heterodyne detection of low-energy vibrations and identification of excited-state
contributions
APL Photonics **4**, 056102 (2019); https://doi.org/10.1063/1.5090585

Attosecond pulse metrology Ⓕ

View Online   Export Citation   CrossMark

I. Orfanos,[1,2] I. Makos,[1,2] I. Liontos,[1] [iD] E. Skantzakis,[1] [iD] B. Förg,[3,4] D. Charalambidis,[1,2] and P. Tzallas[1,a]

AFFILIATIONS

[1] Foundation for Research and Technology - Hellas, Institute of Electronic Structure & Laser, P.O. Box 1527,
GR71110 Heraklion (Crete), Greece
[2] Department of Physics, University of Crete, P.O. Box 2208, GR71003 Heraklion (Crete), Greece
[3] Max Planck Institute of Quantum Optics, Garching, Germany
[4] Department of Physics, Ludwig-Maximilians-Universität München, München, Germany

[a] Author to whom correspondence should be addressed: ptzallas@iesl.forth.gr

ABSTRACT

The long-standing scientific quest of real-time tracing electronic motion and dynamics in all states of matter has been remarkably benefited by the development of intense laser-based pulsed sources with a temporal resolution in the attosecond [1 attosecond = 10^{-18} s] time scale. Nowadays, attosecond pulses are routinely produced in laboratories by the synthesis of the frequency components of broadband coherent extreme ultraviolet (XUV) radiation generated by the interaction of matter with intense femtosecond (fs) pulses. Attosecond pulse metrology aims at the accurate and complete determination of the temporal and phase characteristics of attosecond pulses and is one of the most innovative challenges in the broad field of ultrashort pulse metrology. For more than two decades since coherent high-brilliance broadband XUV sources have become available, fascinating advances in attosecond pulse metrology have led to the development of remarkable techniques for pulse duration measurements as well as the complete reconstruction of those pulses. Nonetheless, new challenges born from diverse fields call upon for additional efforts and continuously innovative ideas in the field. In this perspective article, we follow the history of ultrashort pulse technology tracing attosecond pulse production and characterization approaches, focus on the operation principles of the most commonly used techniques in the region where they interact with matter, address their limitations, and discuss future prospects as well as endeavors of the field to encounter contemporary scientific progress.

I. HISTORICAL OVERVIEW

A. Chronoscopy of ultrashort pulse technology advances

The complete description of light-matter interaction was always considered to be one of the most challenging tasks for the scientific community as it involves the understanding of the coupled dynamics of the building blocks of matter such as nuclei, electrons, and photons. The measurement of short time intervals and the perception of the dynamics of the microcosm are largely dependent on tools used for tracing these dynamics. Such tools are the light pulses used to trigger and detect, via nonlinear processes, the evolution of the systems in the microcosm. The need for finer time resolution and the quest for higher peak power underlie the continuous efforts toward shorter laser pulses almost since the inception of the laser.

The historical progress of ultrashort pulse technology is summarized in Fig. 1.

In the 1960s, the breakthrough of the invention of Continuum Wave (CW) lasers[1] meant to change the course of history on light technology and light–matter interactions. Countless fascinating discoveries and applications are based on the coherent properties of these light sources and their linear interaction with matter. Almost a decade after the discovery of CW lasers, the development of nanosecond (ns) pulsed laser sources[2] allowed the scientific community to enter the nonlinear light-matter interaction regime. Due to the low (relative to the Coulomb field of the atomic potential) electric field of these laser pulses, the interaction can be treated by the lowest-order perturbation theory. Only with the development of shorter pulses, picosecond (ps)[3] and especially the femtosecond[4,5] laser systems [combined with the chirped-pulse amplification
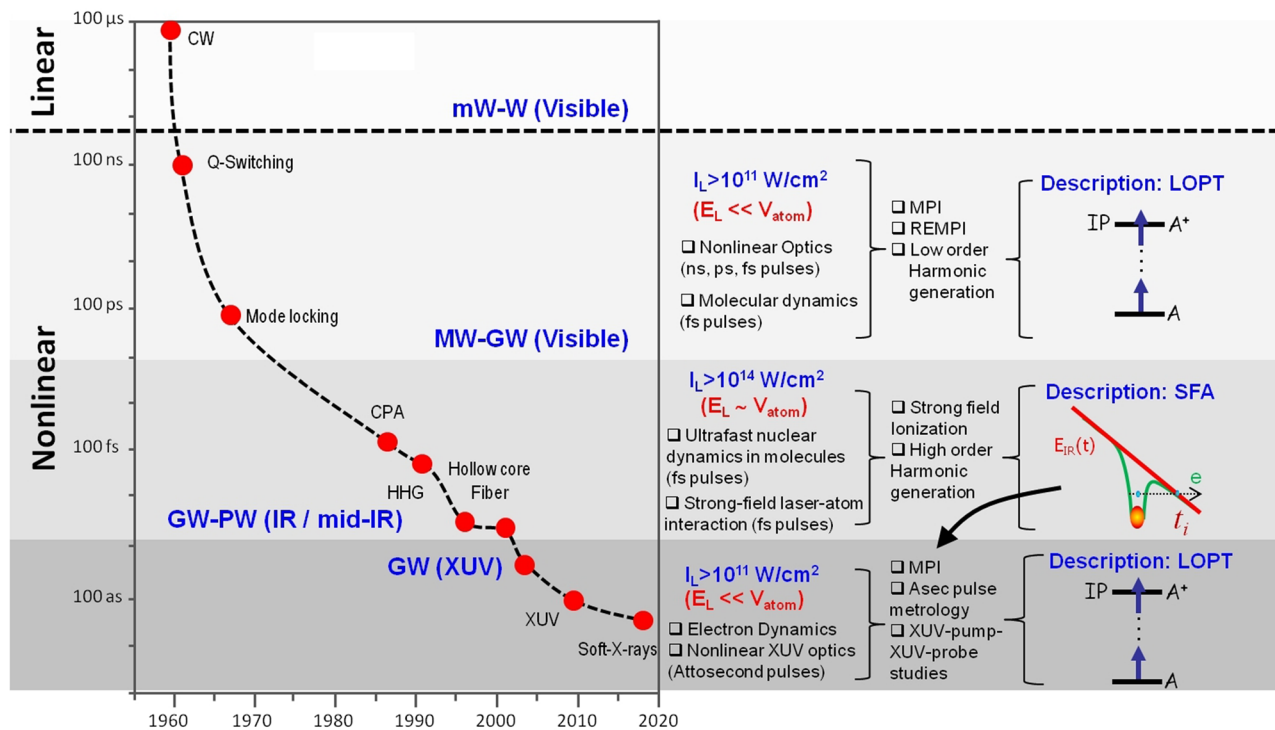
FIG. 1. Historical progress of the ultrashort pulse technology. E_L: laser electric field; V_{atom}: atomic potential; MPI: multiphoton ionization; REMPI: resonance enhanced multiphoton ionization; LOPT: lowest-order perturbation theory; SFA: strong field approximation; and E_{IR}: electric field of the infrared (IR) laser at the moment of ionization t_i.

(CPA) technology[6,7]] at the end of the 1980s, it became possible for the scientific community to access ultrafast molecular dynamics in the time domain[8] and perform studies beyond the perturbative regime. In this strong-field regime, the system is exposed to laser electric fields comparable to or stronger than the field of the atomic potential. The latter had a tremendous impact on atomic and molecular physics and eventually led to the development of the semiclassical "three-step" model[9–11] underlying the generation of high harmonics (HH)[12–14] and attosecond science,[15–19] which have been recently linked with quantum optical technology[20] through the quantum optical description of strongly laser driven interactions.[21–23]

B. Attosecond pulse production

Nowadays, subfemtosecond subcycle electric fields can be synthesized using broadband radiation in the visible spectral range[24] and attosecond pulses are generated in the XUV spectral range.[25,26] Additionally, the recent development of mid-IR few cycle-laser systems led to the generation of coherent soft x-ray radiation[27–29] with the shorter ever measured duration to be ≈43 as.[30] Presently, gases are considered among the most favorable nonlinear media in use for the production of attosecond pulses in the 20–100 eV XUV photon energy regime, yielding photon fluxes ranging from 10^7 to 10^{11} photons/pulse.[31–40] The most recent development with respect to XUV pulse energies is the ≈20 GW XUV beam line constructed at the Attosecond Science and Technology Laboratory of the

Foundation of Research and Technology (FORTH)[39] which delivers XUV pulses with ≈6 × 10^{13} photons/pulse in the spectral region of 20–30 eV.

By focusing intense linearly polarized multicycle femtosecond driving laser pulses [Fig. 2(a)] on gases, an XUV frequency comb, consisting of the HH of the driving laser frequency ω_L [Fig. 2(b)], is emitted in the direction of the laser propagation. Under proper phase matching conditions, the phase locking between the harmonics forms an attosecond pulse train (APT) [Fig. 2(c)]. The overall duration of the train is limited by the average bandwidth of the individual harmonics, while the duration of the attosecond pulses in the train is limited by the full bandwidth of the XUV harmonics spectrum. Confining the High-Harmonic Generation (HHG) process to occur within a fraction of the cycle of the driving laser field [Fig. 2(d)] may lead to the production of an Isolated Attosecond Pulse (IAP) and with a continuum spectral power distribution [Fig. 2(e)]. The shortest duration of an IAP is limited by the bandwidth of the continuum XUV spectrum [Fig. 2(f)]. Examples of attosecond beam line arrangements can be found in Refs. 25 and 40–48.

C. Repertoire of attosecond pulse characterization approaches

Despite the tremendous progress in attosecond pulse engineering over the last 20 years, attosecond pulse metrology is still one of the most challenging research directions. Independent of the high
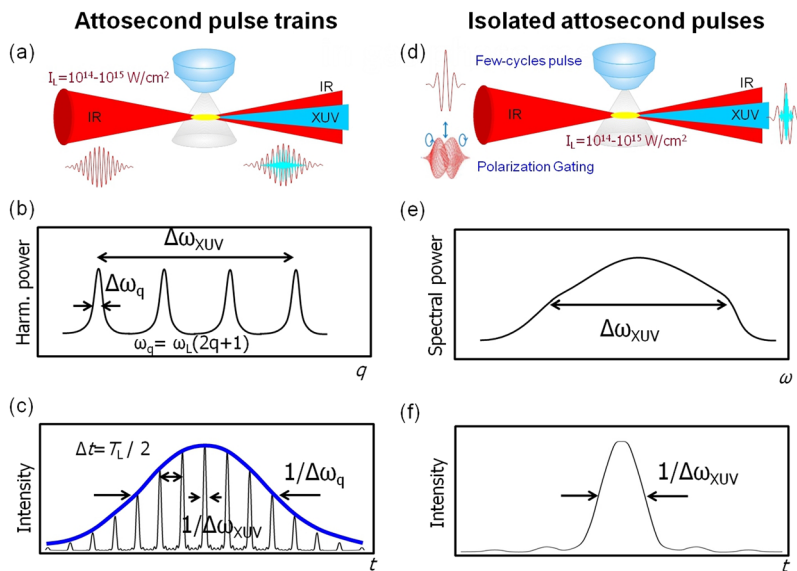
FIG. 2. Schematic representation of the attosecond pulse generation in gas phase media. q is the harmonic order, ω_q is the harmonic frequency, ω_L is the laser frequency, T_L is the period of the laser cycle, ω_{XUV} is the carrier frequency of the XUV pulse, $\Delta\omega_q$ is the harmonic bandwidth, and $\Delta\omega_{XUV}$ is the bandwidth of the XUV pulse.

harmonic source used for synthesizing the attosecond pulses, the difficulty in conducting pulse characterization experiments arises from the inherently low reflectivity, the high absorption/dispersion of the XUV optics, and the lack of spectrally flat with instantaneous temporal response materials. These factors make the use of nonlinear crystals and conventional beam splitters not feasible for experimental implementation, hence preventing the direct translation in the XUV spectral domain of conventional techniques employed for temporal characterization of ultrashort pulses in the visible and near-infrared (IR) spectral regions. However, notable methods for attosecond pulse characterization have been implemented owing to the continuous scientific advances in both ultrafast light-matter interaction and engineering in the XUV spectral range. These methods can be divided into two main categories: those that are based on cross correlation (CC) and the ones based on nonlinear volume autocorrelation (AC) approaches; both characterize the attosecond pulses in the region where they interact with matter. In situ[49,50] and Spectral Phase Interferometry for the Direct Electric Field Reconstruction (SPIDER)[51,52] methods have also been developed. The former provides information about the attosecond pulses at the point of their generation, while the latter utilizes generation of harmonics from two different sources with slightly shifted central frequency, assuming identical harmonic generation in these two sources. In addition, a conceptually new all-optical approach has been recently demonstrated experimentally.[53] The method is stimulated by double-blind holography and is based on the spectral measurement of two unknown XUV-attosecond pulses and their interference.

The AC approach[40,54–56] (which requires high XUV intensities $>10^{11}$ W/cm^2) relies on the interaction of two parts of the pulse to be characterized that are considered to be identical and results in a direct measurement of the pulse duration. The approach was used for the temporal characterization of attosecond pulses generated in gases[34,54,57,58] and solid-surfaces.[59] The same experimental setup has been employed for XUV-pump-XUV-probe studies of the 1-fs

electron dynamics of atoms/molecules[34,35,60–62] and time delay spectroscopic studies in atoms.[63] As has been stated before, the implementation of AC experiments and measurements in the XUV by means of nonlinear crystals is hindered by the absence of suitable optics in this spectral region and so far, remains an open challenge. On the contrary, AC measurements can be accomplished by recording ions or photoelectrons (PEs) induced by two-photon ionization processes in an appropriate target medium. In this context, several materials and ionization schemes have been proposed and explored, such as two-photon ionization of helium,[54,64] two-photon above-threshold ionization (ATI) of helium,[55,59,65] two-photon double ionization of helium, and two-photon ATI of argon.[65,66] In all cases, ions or PEs are collected using appropriate ion or electron time-of-flight (TOF) spectrometers, respectively. A dispersionless Michelson-type interferometer for AC measurements using two identical replicas of the XUV pulses has been developed and modeled.[67] Due to the high losses that it introduces to the XUV radiation, it has been used so far only in the UV spectral region.[68–70]

In contrast to AC, the CC approaches relax the requirement of high XUV intensities but they do not provide direct information (in the sense that a second field is needed for the characterization) on the pulse duration. They rely on the reconstruction of the pulse which occurs after analyzing the data obtained by the interaction of atoms with the superposition of the XUV pulse with an IR field. These principles have been incorporated in the following schemes. The Reconstruction of Attosecond Beating By Interference of two-photon Transitions (RABBIT) technique[71] (applicable for APTs) uses the fundamental laser field to create sidebands in the photoelectron (PE) spectra generated by the XUV harmonics. The average duration of the pulses within the attosecond pulse train can be deduced by recording the products of the quantum interference of different two-photon (XUV and IR) ionization channels. Another technique known as attosecond streak camera [applicable for isolated attosecond pulses (IAPs) and free-electron laser (FEL) light sources][72–74] uses the fundamental electric field to

modulate the energy distribution of the PEs generated by the XUV photons. This modulation was used to determine the duration of the IAP[72,75,76] and has subsequently also been applied to study the attosecond dynamics in gases[77,78] as well as solids.[79] The tool box of CC approaches also contains a technique named Frequency Resolved Optical Gating for Complete Reconstruction of Attosecond Bursts (FROG-CRAB) which is applicable for arbitrary attosecond fields[80] and a technique named Phase Retrieval by Omega Oscillation Filtering (PROOF) which is applicable for arbitrary attosecond fields with bandwidth >70 eV.[81] An advanced version of the RABBIT technique is the so-called RAINBOW RABBIT,[82,83] which detects frequency resolved CC interaction products, thus allowing the study of subtle phenomena not attainable by RABBIT. In Secs. II–VI, we will review these approaches restricting ourselves to methods capable of characterizing attosecond pulses generated by a single source and detected in the region of their interaction with matter.

II. AUTOCORRELATION APPROACHES

After a brief introduction in the nonlinear processes employed in the autocorrelation approaches, we describe the second-order intensity volume autocorrelation (2-IVAC) approach used for the temporal characterization of attosecond pulse trains and isolated pulses. Then, the XUV-FROG applications are discussed as well as how the XUV-FROG technique is used to retrieve the phase and fully reconstruct APTs and IAPs, respectively.

A. Nonlinear ionization processes

In order to conduct a 2nd order AC measurement in a gas medium with confidence, it is of paramount importance to verify that the two-photon process dominates the gas ionization and hence, is suitable for second-order AC. First, it should be confirmed that the focused intensity at the point of interaction with the gas target is adequately high and capable of producing a recordable number of ions or electrons induced by two-photon ionization (Fig. 3).
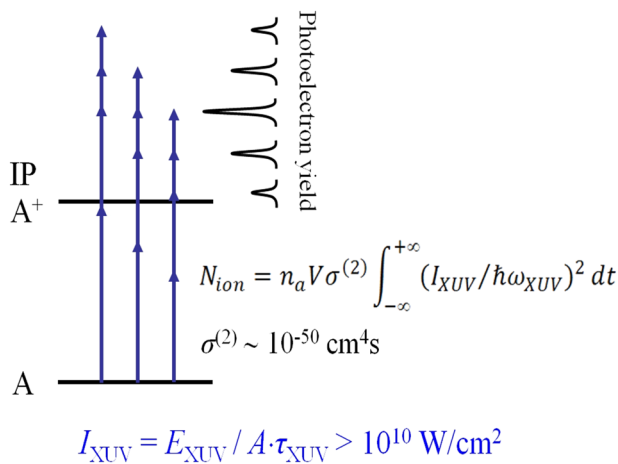

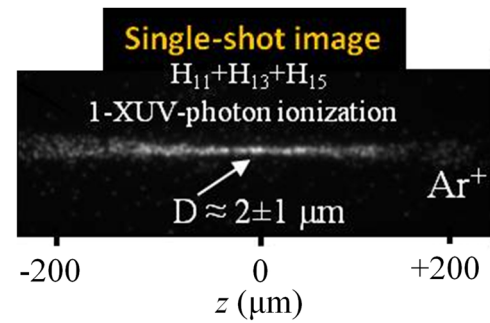FIG. 3. Two-XUV-photon ionization scheme of an atom A. IP is the ionization potential of A.

Therefore, one must make a calculated estimation, under realistic experimental conditions, of the two-XUV-photon nonresonant ionization yield (Y_2) (ions/electrons), and hence the XUV intensity (I_{XUV}) that would be sufficient to induce such a nonlinear atomic process. The transition probability rate W_2 and the Y_2 per pulse for a two-photon absorption process are given by $W_2 = \sigma^{(2)}(I_{XUV}/\hbar\omega_{XUV})^2$ and $Y_2 = W_2\tau_{XUV}n_aV$, respectively; n_a is the atomic density at the volume V of interaction and $\sigma^{(2)}$ is the generalized two-photon ionization cross section with values ranging from 10^{-49} to 10^{-52} cm^4 s. Taking into account typically reached experimental atomic densities of ~10^{15} atoms/cm^3 and an interaction volume of ~$V = 10^{-9}$ cm^3, then a recordable two-photon ionization yield would require $I_{XUV} > 10^{10}$ W/cm^2.

Ions and photoelectrons produced by a two-XUV-photon nonresonant[84] ionization process have been observed using XUV pulses in the nano-Joule energy range.[54,56,63,85–88] The spatial characteristics of the XUV beam at the interaction region can be obtained experimentally by means of an Ion Microscope (IM).[89–91] Figure 4 shows an example of the spatial distribution of the XUV radiation at the focus recorded in a single shot.

Apart from the measurement of the XUV beam spatial characteristics in the interaction region, the IM can also be used in obtaining quantitative information about generalized cross sections in the linear and nonlinear XUV spectral regions.[89,90,92]

B. Operation principle of the 2-IVAC

The 2-IVAC approach was first demonstrated in 2003[54] using gas phase harmonics and in 2009 using harmonics emitted from laser-plasma interactions.[59,93] Autocorrelation measurements in the visible/infrared spectral region are based on the interference between two cotraveling replicas of the pulse created by a beam splitter and separated in time by adding the optical path to one of the arms corresponding to various time delays in their propagation. However, since no conventional dispersionless beam splitter is available for XUV wavelengths, the two XUV pulses are created using an XUV wave front splitting device. Such a device is a split spherical mirror where one of the two-halves is fixed and the other is
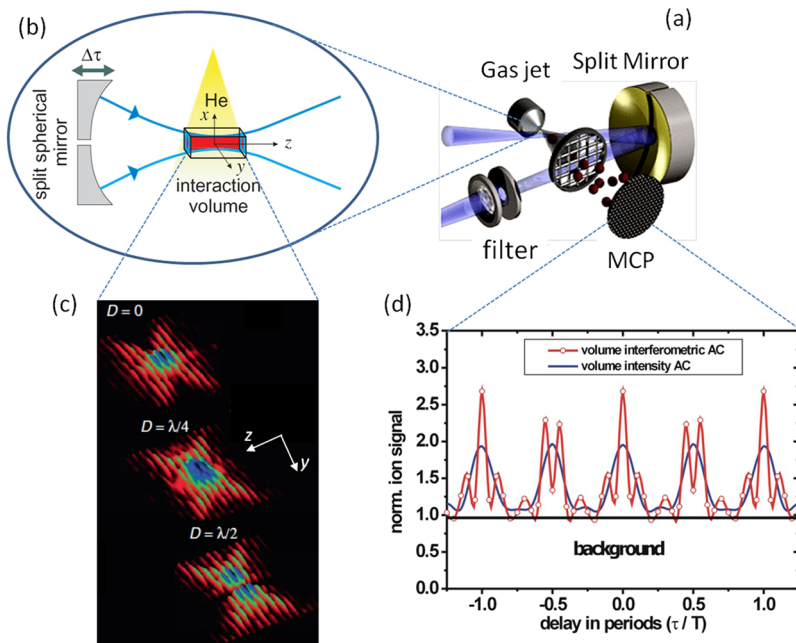
FIG. 5. (a) Schematic of the experimental setup of the second-order XUV volume autocorrelator utilizing the split mirror configuration. (b) Interaction volume in the case of using He gas as a two-photon detector. (c) Two-dimensional (z–y) contour plots showing the snapshots of the calculated intensity distribution of the harmonic superposition (7th + 9th + 11th + 13th) in the interaction region of the volume autocorrelator for displacement D = 0, D = λ/4, and D = λ/2 between the two pulses. (d) Calculated interferometric and intensity volume autocorrelation traces. T is the period of the IR laser field. In these calculations, the peak to background ratio of the interferometric trace is $\approx$2.75:1 with the cycle average resulting in a ratio of $\approx$2:1.[56] However, detailed calculations performed in 2009[94] for the 5th harmonic, which have been confirmed experimentally,[94,96] have shown that the peak to background ratio and the interferometric and intensity volume autocorrelation ratio are $\approx$3.4:1 and $\approx$2.4:1, respectively. (b)–(d) Reprinted with permission from Charalambidis *et al.*, *Progress in Ultrafast Intense Laser Science*. Copyright 2009 Springer Nature. Reprinted with permission Springer Nature.[97]

on a piezotranslation stage [Fig. 5(a)]. This device provides a solution to the introduction of a variable time delay between the two pulses not only for pulse duration measurements but also for XUV-pump–XUV-probe experiments in atoms and molecules. Using the nonlinear ionization schemes described in Sec. II A, the autocorrelation trace results in measuring the ionization products (electrons or ions) recorded by a TOF spectrometer as a function of the delay.

The operation principle of the 2-IVAC relies on the spatial integration of 2-XUV-photon ionization yield produced in the interaction volume [Fig. 5(b)] by the coherent superposition of the two XUV pulses created by the XUV wave front divider[54,56] (additional information can be found in Refs. 94 and 95).

For attosecond pulses synthesized from the harmonics 7th, 9th, 11th, and 13th, the field distribution is given by $E(D, x, y, z) = \sum_{n=7}^{n=13} E_n(D, x, y, z)$ (D is the displacement introduced by the delay stage between the two XUV pulses) at the focal spot of the focusing element. The projection of the intensity distribution $I(D, x, y, z) = E(D, x, y, z)E^*(D, x, y, z)$ on the z-y plane for the particular values of the displacement D = 0, λ/4, and λ/2 is shown in Fig. 5(c). The beam profile is an airy distribution in the focus, and for a displacement of D = λ/2, it is divided into two parts of equal size. It is worth noting that the total energy in the interaction volume remains constant, and as a result, the splitting of the focal spot would not affect the measured signal (integrated over the whole interaction volume) in the case of single photon ionization (linear detector), i.e., the signal would remain constant at all time delays. In the case of two-photon ionization (quadratic detector), a modulation in the ionization signal $S(D) \propto \iiint_{\Delta V} I^2(D, x, y, z)dxdydz$ would occur due to the rearrangement of the local intensity inside the interaction volume. The blue and red curves in Fig. 5(d) correspond to the calculated two-photon intensity and interferometric volume autocorrelation, respectively.

The peak-to-background ratio in the 2nd-order interferometric volume autocorrelation is $\approx$3.4:1 and in the 2nd-order intensity volume autocorrelation is $\approx$2.4:1.[94] The attosecond pulse duration τ_{XUV} can be determined from the measured autocorrelation trace (AC) using the well-known relation valid for Gaussian pulses $\tau_{XUV} = \tau_{AC}/\sqrt{2}$ (where τ_{AC} is the full width at half maximum of the AC trace). At this point, it should be noted that the measured pulse duration, in the case of pulse trains, reflects the average duration of the individual attosecond pulses composing the train.

C. 2-IVAC in attosecond pulse trains and isolated attosecond pulses

2-IVAC pulse duration measurements of an APT as well as of an isolated ~1 fs XUV pulse are shown in Figs. 6(b) and 6(c) and [Figs. 6(d) and 6(e)], respectively. A common experimental apparatus has been used for both cases, which is drawn in Fig. 6(a). For the production of the APT, a high-power multicycle femtosecond IR pulse is focused on a xenon gas jet target. The focusing position of the driving field was set before the xenon gas jet, a position which experimentally is considered to be favorable for temporal confinement in the attosecond scale. The latter is attributed to the phase accumulated by the ejected electrons following a short trajectory before recombining with the parent ion. A 150 nm-thick indium foil filter selects the 9th to 15th odd harmonics with the relative field amplitudes in the interaction region to be 1, 0.4, 0.3, and 0.25 for the 9th, 11th, 13th, and 15th harmonics, respectively. By focusing the radiation on a helium pulsed gas jet using a split spherical gold mirror of 5 cm focal length, the 2-XUV-photon ionization process was observed and single-charge helium ions [Fig. 6(b)] were collected utilizing a μ-metal-shielded time-of-flight (TOF) spectrometer. The experimental 2-IVAC trace obtained by recording the He$^+$ signal as
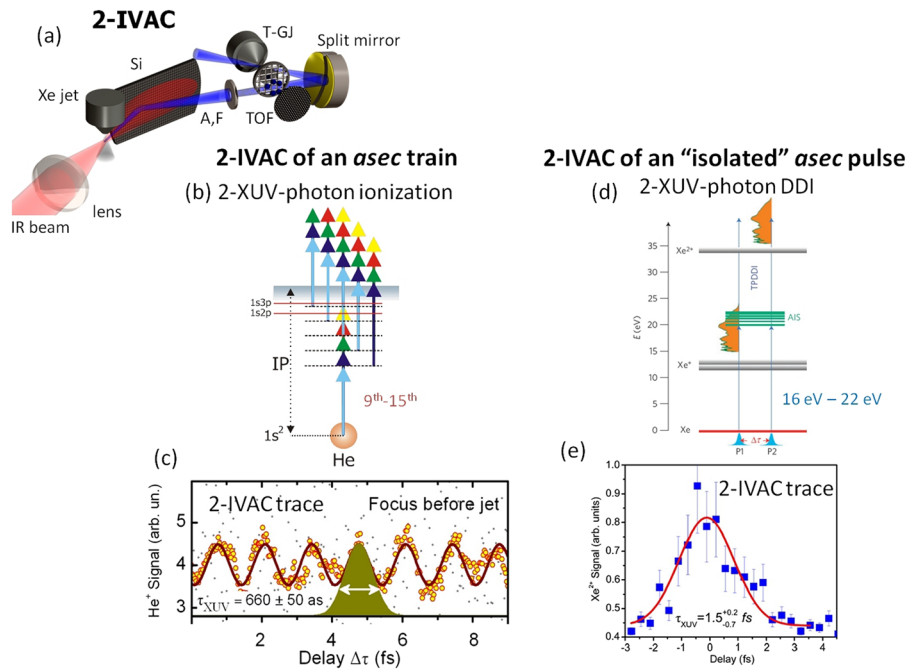
FIG. 6. (a) Experimental setup. (b) 2-XUV-photon ionization scheme of helium using the 9th–15th harmonics passing through indium filter. (c) 2-IVAC trace of an APT synthesized by the 9th–15th harmonics. Gray dots are the raw data, and the yellow correspond to a 10-point running average. The purple line is a 12-peak sum of Gaussians fit to the raw data. (d) 2-XUV-photon direct double ionization (TPDDI) scheme of xenon using the broadband coherent continuum XUV radiation (orange filled areas) generated in a xenon gas jet by means of PG arrangement. In this process, the single XUV photon absorption is passing through an ensemble of autoionizing states (AIS). (e) 2-IVAC trace. The blue squares are the raw data, and the red line is a Gaussian fit to the raw data. The pulse broadening is a consequence of the appearance of side pulses due to the unstable carrier-envelope-phase (CEP) of the high-power multicycle laser system. (c) Reprinted with permission from Kruse et al., Phys. Rev. A **82**, 021402(R) (2010). Copyright 2010 American Physical Society. (d) Reprinted with permission from Tzallas et al., Nat. Phys. **7**, 781 (2011). Copyright 2009 Springer Nature. (e) Reproduced with permission from P. Tzallas, E. Skantzakis, and D. Charalambidis, J. Phys. B: At. Mol. Opt. Phys. **45**, 074007 (2012). Copyright 2012 IOP Publishing. All rights reserved.

a function of the time delay between the XUV replicas is shown in Fig. 6(c). The average duration of attosecond pulses within the pulse train was found to be 660 ± 50 as.[98]

Volume autocorrelation measurements can be carried out not only for the characterization of APTs but also for IAPs, which are more suitable for pump-probe experimental schemes in attosecond time scale. For the setup sketched in Fig. 6(a), IAPs are produced, using a many-cycle laser field, with the Polarization Gating method (PG), presented in more detail in Refs. 100 and 101. In this case, the generated XUV spectrum is not a comb, like in APTs, but rather a continuum or quasi continuum depending on the CEP variation. Experimental manifestation of the IAP characterization has been presented in Ref. 34 implementing similar configuration as described above for the APT. The XUV radiation was spectrally selected by a 150 nm-thick Sn filter allowing transmission of photon energies centered at ≈19 eV with a bandwidth of ≈10 eV [orange filled area in Fig. 6(d)]. The generated IAPs are focused by an f/5 cm split spherical gold mirror on xenon pulsed gas target up, where up to Xe^{2+} ions were observed by means of a TOF ion mass spectrometer. Doubly charged ions are produced by a 2-XUV-photon direct double ionization process (TPDDI) [Fig. 6(d)]. In this excitation pathway, single-XUV-photon absorption occurs in a continuum that is rich in structure by the presence of an ensemble of autoionizing states (AIS), which are eventually coherently excited.

The 2-IVAC trace obtained by recording the Xe^{2+} signal as a function of the delay between the XUV replicas is shown in Fig. 6(e). For longer delay times, and acting like an XUV-pump-XUV-probe scheme, information about the wave packet evolution induced by the atomic coherences can be extracted. The obtained temporal duration of the XUV pulse was $\approx 1.5^{+0.2}_{-0.7}$ fs. This result is an overestimation of the actual pulse duration, mainly due to the unstable CEP of the high-power multicycle driving laser pulses which leads to a double pulse structure of the generated XUV. The latter effect is exhibited by the presence of side peaks in the 2nd order AC trace, which due to the lack of resolution cannot be resolved and thus determined.[99] It should be noted that the effect the AIS have in the measured pulse duration can be safely neglected since the width of the states is much smaller than the bandwidth of the XUV pulse or equivalently the measured beating periods are significantly larger than the pulse duration. A more detailed discussion on this topic can be found in Refs. 34 and 84.

The first interferometric volume autocorrelation trace of an APT has been demonstrated in 2006.[102] Using a two-XUV-photon ionization process induced in N_2 upon interaction with an APT which was formed by the 9th–19th harmonics of a driving 40 fs IR laser pulse. The AC trace was obtained by measuring N^+ {resulting from the Coulomb explosion of N_2 after absorbing two-XUV-photons [Fig. 7(a)]}, as a function of the delay between the two XUV
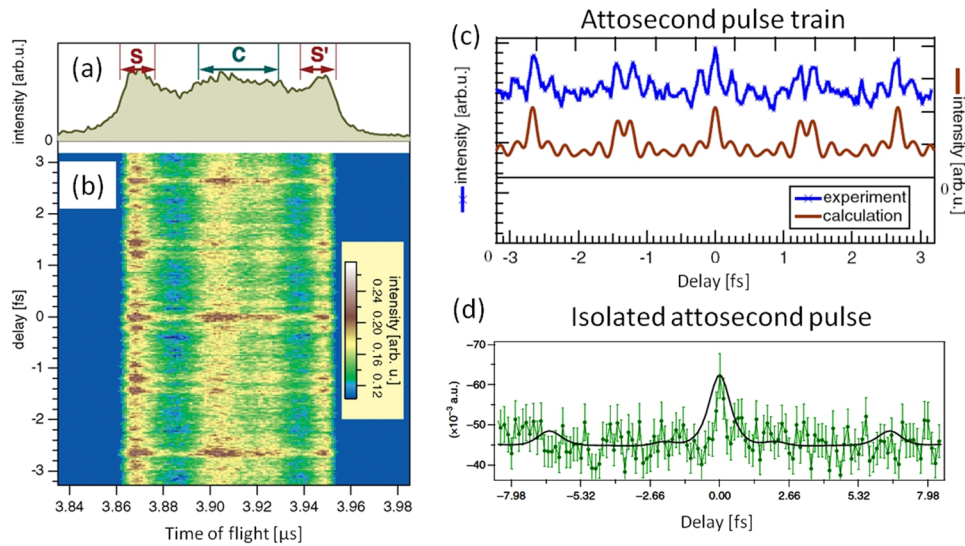
FIG. 7. Left panel: time-of-flight mass spectrum at $m/e = 14$. (a) Typical spectrum of ions originating from a N_2 molecule with two-photon absorption of high-order harmonic fields. (b) Variation of the spectrum by translating the delay between the two pulses of the harmonic fields. Bunches with a period of 1.33 fs and fringes with a much shorter period reveal the interferometric autocorrelation of the harmonic fields. The color scale of the intensity is shown in the inset. (c) Interferometric autocorrelation trace of the APT resulted from the data analysis of (b) (blue line). The calculated correlation trace is shown as the lower curve (orange line). (d) Autocorrelation trace of an IAP obtained following the approach used to obtain the trace the APTs. (a)–(c) Reprinted with permission from Nabekawa *et al.*, Phys. Rev. Lett. **97**, 153904 (2006). Copyright 2006 American Physical Society. (d) reprinted with permission from Takahashi *et al.*, Nat. Commun. **4**, 2691 (2013). Copyright 2013 Springer Nature.

pulses [Fig. 7(b)]. The same approach was used to measure the duration of an IAP in the spectral range around ≈31 eV and a bandwidth of ≈9 eV.[36]

D. XUV FROG-type measurements

The work in Ref. 57 presents a mode-resolved autocorrelation technique applied for the determination of the temporal duration of attosecond pulses. It introduced the use of the 2-IVAC approach through 2-XUV-photon above-threshold-ionization (ATI) schemes,

opening up the possibility of extending the applicability of 2-IVAC to high XUV photon energies and enabling FROG-type[103] measurement. It is considered to be the proof-of-principle experiment of the XUV FROG-type technique. In Ref. 57 isolated XUV pulses with photon energy ≈28 eV (9th harmonic of a 400 nm driving laser field) and bandwidth of ≈2 eV have been generated by the interaction of argon gas phase atoms with ≈8.3 fs driving laser field of carrier photon energy at 3.1 eV. Two optically delayed replicas of the XUV pulse were focused on helium gas inducing a 2-XUV-photon ATI ionization [Fig. 8(a)].

FIG. 8. (a) 2-XUV-photon ATI process of He using isolated XUV pulses with central photon energy ≈28 eV and bandwidth of ≈2 eV. The XUV pulses were generated by the interaction of argon gas with a ≈8.3 fs long driving laser field of carrier photon energy at 3.1 eV. (b) Produced photoelectron spectrum. The ATI peak is shown in red. (c) Recorded AC trace (black points). The red line shows the Gaussian fit on the raw data. Reprinted with permission from Sekikawa *et al.*, Nature **432**, 605 (2004). Copyright 2004 Springer Nature.
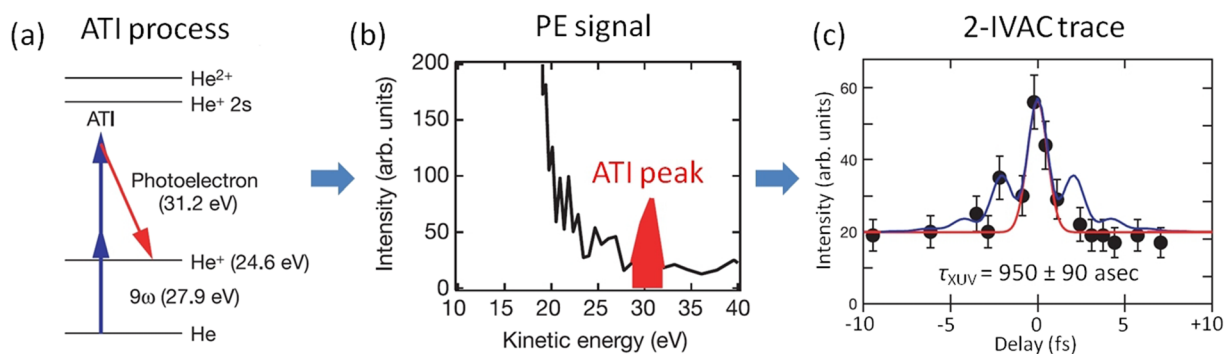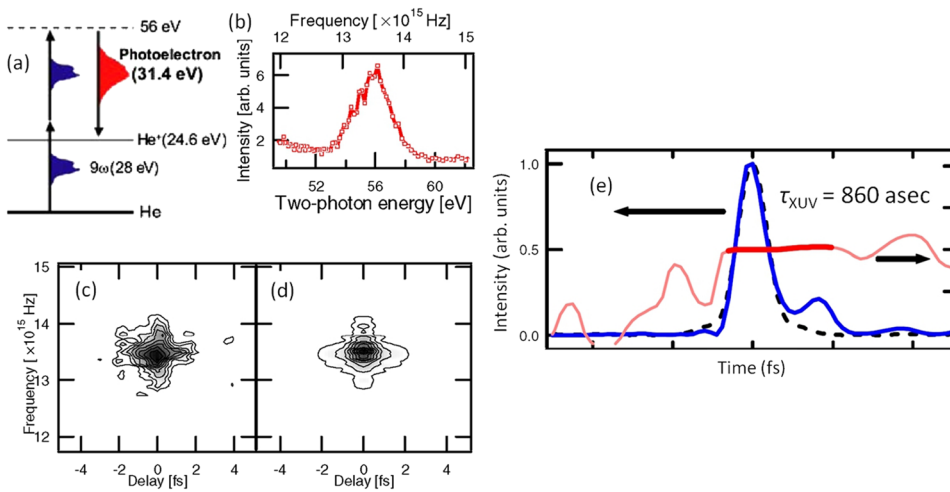
FIG. 9. (a) 2-XUV-photon ATI process of He using isolated XUV pulses with central photon energy ≈28 eV and bandwidth ≈2 eV. (b) Recorded 2-XUV-photon ATI photoelectron spectrum. (c) Measured time-frequency map of the spectrum vs time delay between two replica of the ninth harmonic pulses. (d) Time-frequency map retrieved from (c) by the iterative Fourier-transform algorithm with generalized projection. (e) Retrieved pulse shape and spectral phase distribution. Reprinted with permission from Kosuge *et al.*, Phys. Rev. Lett. **97**, 263901 (2006). Copyright 2006 American Physical Society.

The ejected photoelectrons were collected and energy-resolved by a magnetic bottle photoelectron spectrometer. Figure 8(b) shows the photoelectron spectrum of two-photon ATI. An autocorrelation trace having an overall width of ≈4 fs was recorded by measuring the electron number at each optical delay between the two XUV pulses [Fig. 8(c)]. A Gaussian fit on the central part of the trace resulted in an XUV pulse duration of 950 as. A relatively low experimental spectral resolution prevented a FROG-type analysis, but it sparked additional experimental efforts which proved to be fruitful soon after.

To our knowledge, the only existing XUV FROG-type measurement of an isolated subfemtosecond XUV pulse is the one reported in 2006.[58] This has been achieved by recording with high energy resolution (~200 meV) autocorrelation traces of a two-XUV-photon ATI photoelectron peak. The relevant two-XUV-photon ATI process is drawn in Fig. 9(a), while [Fig. 9(b)] shows the recorded PE ATI peak. The FROG traces are presented in Figs. 9(c) and 9(d) and the retrieved XUV pulse in Fig. 9(e). The duration of the retrieved isolated pulse was found to be 860 as.

In Ref. 57, an experimental technique is introduced for XUV FROG-type attosecond pulse train characterization, termed PANTHER (Photoelectron Analysis with Nonresonant Two-photon-ionization for Harmonic Electric-field Reconstruction). It is a two-photon volume autocorrelation approach mediating through a two-XUV-photon ATI scheme (a process treated according to the lowest-order perturbation theory) in argon gas. By recording autocorrelation traces of energy-resolved ATI photoelectrons, and in combination with FROG-based considerations analysis, the authors managed to retrieve the chirp, among the involved harmonic fields forming the APT, and obtain an upper bound of 450 as for the temporal duration of the APT.

III. CROSS CORRELATION APPROACHES

The following techniques were proposed and implemented for the complete, *phase and amplitude*, characterization of attosecond pulses, as knowledge of both parameters allows obtaining the full picture for the temporal intensity distribution of the pulses. They

are based on the measurement of the photoelectron spectrum produced in gaseous media by their interaction with an XUV attosecond field in the presence of a copropagating femtosecond IR field, as a function of the time delay between the XUV and IR pulses.

A. RABBIT

The RABBIT method aims at characterizing an APT in phase and amplitude. The birth of RABBIT (Reconstruction of Attosecond Beating By Interference of Two-photon Transitions) is traced back in 2001 when Paul *et al.*[71] through their groundbreaking experiment introduced the technique, following the pivotal theoretical work by Véniard *et al.* in 1996.[104] Since then, the approach has been routinely employed in the spectral phase characterization of harmonics and the resulting attosecond pulses (Refs. 105–111).

1. Operation principle of RABBIT

The operation principle of RABBIT is based on the recording of the photoelectron spectrum induced by two-photon two-color ionization (e.g., one-XUV + one-IR photon) of the target medium, e.g., a gas phase noble atom, as a function of the time delay between the XUV attosecond pulse train and the IR fs pulses. A general RABBIT scheme is shown in Fig. 10. If the XUV harmonic comb photon energy exceeds the atomic ionization potential of the experimental target, interaction of atoms with the XUV leads to a photoelectron energy spectrum comprising peaks assigned to single-photon ionization induced by the different harmonic orders of the comb. The attosecond pulse characteristics will be imprinted onto the produced electron wave packet modified by the ionization cross section and the atomic phase. This property is of particular importance when photoemission dynamics, i.e., atomic delays, are to be extracted.[112–114]

Since harmonics are produced at every half optical cycle, the peaks are evenly spaced at $2\hbar\omega_L$ distance, with $\hbar\omega_L$ being the photon energy of the driver laser field. When the second color, usually a weaker (but sufficiently intense) portion of the IR driver pulse, is temporally overlapped with the XUV comb then sideband peaks appear in the photoelectron energy spectrum between the photoelectron peaks solely by the harmonic photons at $\pm\hbar\omega_L$ distances
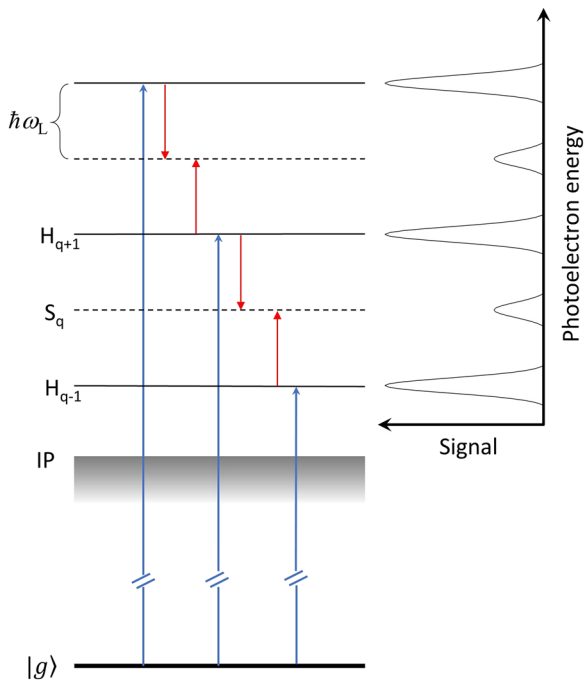
FIG. 10. Ionization scheme of RABBIT. Two-color two-photon ionization of an atom with a ground state $|g\rangle$, by an XUV frequency-comb with a harmonic spacing of $2\hbar\omega_L$ and a synchronized probe field of angular frequency ω_L. In the presence of the probe field, two pathways lead to the formation of sidebands (here, q denotes the sideband order) as depicted in the photoelectron energy spectrum.

from the peaks. Sidebands stem from two-photon two-color ionization, namely, one-XUV photon and absorption or emission of an additional IR photon (Fig. 10).

These continuum states are not excited in the absence of the IR field, a beneficial condition as the measurement can be performed essentially background free. Provided that the IR intensity is weak enough so no multiphoton ionization of the target due to IR occurs, and only one IR photon may be absorbed or emitted,[71] then there are two possible pathways, i.e., two consecutive harmonics, contributing to each sideband. As the temporal delay between the XUV and IR pulses is varied, the amplitude S of these sidebands exhibits a periodical modulation due to the phase difference between adjacent harmonics,[71]

$$S_q(\tau) \propto \cos(2\omega_L\tau + \Delta\varphi_{q+1,q-1} + \Delta\varphi_q^{at}),\qquad(1)$$

where q is the order of the sideband, ω_L is the carrier wave frequency, τ is the XUV-IR time delay, $\Delta\varphi_{q+1,q-1} = \varphi_{q+1} - \varphi_{q-1}$ is the phase difference between $q + 1$ and $q - 1$ harmonics, and $\Delta\varphi_q^{at}$ is the intrinsic phase difference due to the ionization process itself for the qth sideband.[104] $\Delta\varphi_q^{at}$ is usually negligible compared to $\Delta\varphi_{q+1,q-1}$ but can either be calculated or measured.[115–119] The phase between harmonics $\Delta\varphi_{q+1,q-1}$ can be determined by the Fourier transform of the periodical modulation of S_q as a function of τ. The XUV spectrum is measured by blocking the IR beam, taking into account the ionization cross section σ_n of the gas target, where n is the harmonic order (i.e., related to the sideband order q by $q = n + 1$).

The average attosecond pulse in the APT can then be reconstructed by the relative harmonic spectral amplitudes, A_n, obtained by the XUV spectrum, and the interharmonic phases retrieved by the time delay graph. Finally, the average intensity profile I_{avg} of the attosecond pulse in the APT is calculated by the sum of the individual harmonic fields,

$$I_{avg}(t) = \left|\sum_n A_n e^{-in\omega_L t - i\varphi_n}\right|^2,\qquad(2)$$

where $\varphi_n = \sum \Delta\varphi_{q+1,q-1}$ is the obtained spectral phase distribution for harmonic order n, with n spanning the XUV comb forming the APT. The FWHM of the intensity profile $I_{avg}(t)$ gives the temporal duration of the attosecond pulse.

In the advanced version of RAINBOW RABBIT,[82,83] the measured signal of the sidebands is not energy integrated, thus allowing us to follow signal modulations for different spectral components within the spectral bandwidth of the harmonics. This is not crucial when RABBIT is used for the retrieval of the phase difference of subsequent harmonics for which the "classical" RABBIT is sufficient. However, it may become important when RABBIT is used for the measurement of phases related to the structure and dynamics of the atom, in particular when these phases vary fast within the bandwidth of one harmonic, where the energy integration inherent in the "classical" RABBIT may lead to a smearing of the phase information. Nevertheless, such measurements go beyond the scope of this review.

For the sake of comprehensiveness, it should be mentioned that the RABBIT scheme shown in Fig. 10 is incomplete. Apart from the channels involving absorption of an XUV photon with subsequent absorption/emission of an IR photon, there are channels involving first absorption/emission of an IR photon followed by absorption of an XUV photon leading to the same final continuum state. Thus, there are four interfering channels contributing to each sideband $[(\omega_q + \omega_L), (\omega_{q+1} - \omega_L), (\omega_L + \omega_q), (-\omega_L + \omega_{q+1})]$. Usually the last two $[(\omega_L + \omega_q), (-\omega_L + \omega_{q+1})]$ are being considered negligible[120] as they are far detuned from the eigenstates of the system. However, for the first two channels one-photon absorption, and thus the virtual state of the two-photon ionization process, is in the continuum and thus with many continuum states above and many continuum and bound states below the intermediate virtual state. The opposite sign detuning of these two groups results in two-photon ionization amplitudes with opposite sign and thus in partial cancelation. In the two last channels, all allowed excited states (bound and continuum) are above the intermediate virtual state. Despite far detuned from the eigenstates of the atom, all detunings have the same sign and thus no cancelation is occurring. For the two first channels, the Cauchy principal value in the two-photon ionization transition amplitude together with the contribution of the bound states can be comparable if not smaller than the two-photon transition amplitude in the two last channels. Nevertheless, the presence of two or four interfering two-photon ionization channels does not affect the retrieval of the spectral phase distribution as described above.

2. RABBIT in attosecond pulse trains

For the experimental realization of the technique, a multicycle femtosecond intense laser field is used to produce an XUV APT via high-harmonic generation in a gas medium. A typical setup is illustrated in Fig. 11.

In this arrangement, multicycle IR laser pulses, focused on a Xe gas jet, are used for the XUV harmonic generation. After the Xe jet, a silicon wafer is placed at Brewster angle reflecting the XUV radiation while attenuating the IR field. The XUV radiation is appropriately filtered to select plateau harmonics and both XUV and IR are focused by means of a gold spherical mirror on the target gas jet. The time delay between the XUV and IR is varied by rotating a plate placed in the common beam line path. The two-color (XUV+IR) photoelectron spectra are recorded, for all three different focus positions in the HHG Xe gas jet (focus before jet, on jet, and after jet), by means of a μ-metal shielded time of a flight electron spectrometer [Fig. 12(a)]. It shows peaks corresponding to single-XUV (harmonic)-photon ionization and in between them sidebands corresponding to two-color (XUV+IR) photoionization. Variation of the XUV-IR time delay results in periodical modulation of the sideband peaks. The total electron signal modulation is also exhibiting an oscillation period corresponding to one of the fundamentals, i.e., ~2.7 fs, as expected. From the RABBIT traces, the relative harmonic phases are retrieved [Fig. 12(b)] and the attosecond pulse trains are reconstructed [Fig. 12(c)] for all three focus positions.

B. Attosecond streak camera

RABBIT is a powerful tool of attosecond metrology when dealing with attosecond pulse trains. A different approach has to be

FIG. 11. Typical RABBIT experimental arrangement. Reproduced with permission from Kruse et al., Phys. Rev. A **82**, 021402(R) (2010). Copyright 2010 American Physical Society.
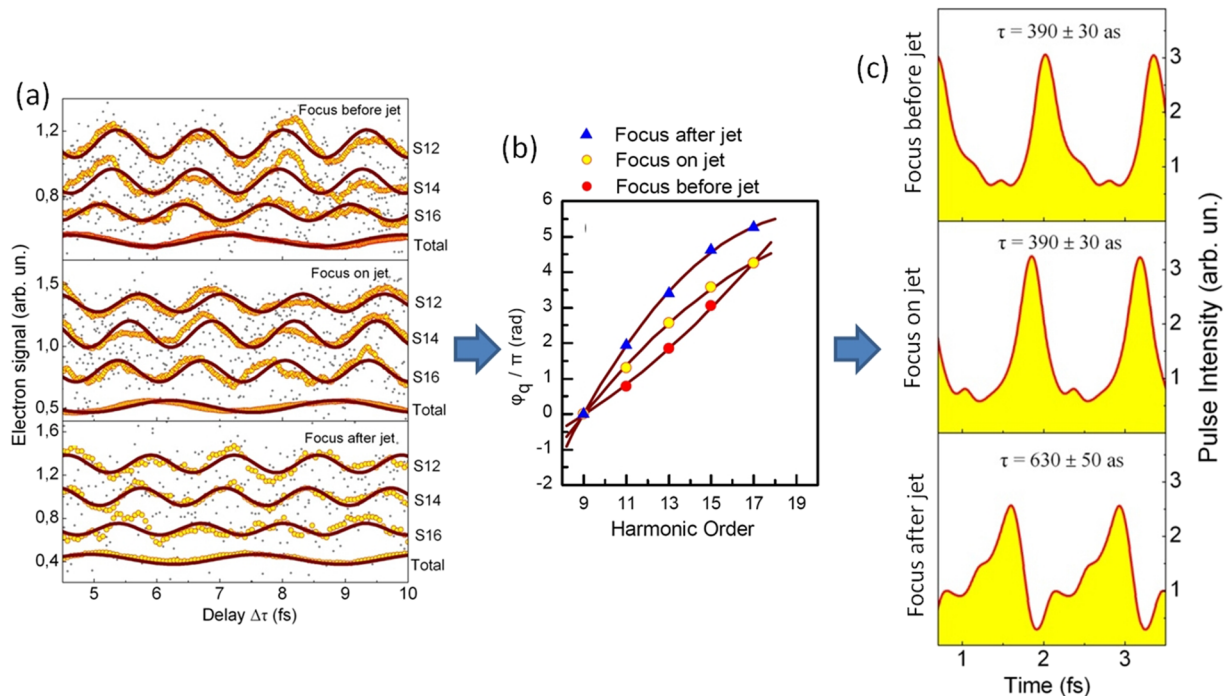
FIG. 12. (a) RABBIT traces at three different positions of the laser focus with respect to the xenon gas jet (focus before jet, focus on jet, and focus after jet) normalized to the corresponding total signal. The gray dots are the measured data, and the yellow circles correspond to a running average of 15 points and 40 points for the total signal. The solid purple lines are sinusoidal fits to the raw data over 13 oscillations on the sideband traces and over 6 oscillations on the total signal. (b) Phases of the consecutive harmonics obtained by the RABBIT traces. (c) Reconstructed APTs. Reprinted with permission from Kruse et al., Phys. Rev. A **82**, 021402(R) (2010). Copyright 2010 American Physical Society.

followed when an isolated attosecond pulse (IAP) comes into play mainly because a harmonic continuum is required for the IAP production. Several different methods for creating IAPs have been realized up to date including amplitude gating,[72,121] ionization gating,[57,122] polarization gating,[123,124] interferometric polarization gating,[100] double optical gating,[125] two-color gating,[126,127] lighthouse,[128] and spatiotemporal gating[129] methods. In all cases, full access to the electric field amplitude and phase of the IAPs is offered by utilizing an experimental technique termed the *attosecond streak camera* formulated around the late 1990s[130,73,74] and demonstrated experimentally for the first time in 2004.[75] Since then, it has been widely applied for the complete characterization of the isolated attosecond pulses.

1. Operation principle of the attosecond streak camera

In a conventional streak camera, the time-varying signal is transformed into a spatial profile on a detector mapping its spatial change when a time-varied deflection is applied on the signal. This concept has been extrapolated in the attosecond streak camera where the role of the time-varied deflection is now being served by a fast-changing, typically few-cycle, IR field which dresses the electron pulse production.

The attosecond streak camera, as a cross correlation technique, relies on the photoionization of a target medium by the XUV IAP in the presence of a synchronized strong IR pulse. Although the initial idea of this method is to measure the photoelectron spectra at specific delays (in principle, one delay is enough), where the laser field streaks the photoelectron energy, and to compare these spectra to the laser-free photoelectron spectrum, traditionally the IAP duration is retrieved by recording a streaking trace obtained by varying the XUV-IR time delay. Both XUV and IR pulses are considered to possess the same linear polarization. The measured electron kinetic energy spectrum can be recorded in various streaking detection angles with the most favorable being the one parallel to the laser polarization axis. Several assumptions are in order,[130] (i) the product of the XUV single photon ionization in the form of an electron pulse is an exact replica of the IAP, i.e., unstructured continuum over the IAP bandwidth, (ii) in the spirit of strong-field approximation, no strong field modification due to XUV occurs, i.e., ground state atoms are promoted directly to the continuum with no intermediate resonances with excited states, and (iii) the IR streaking intensity, typically realized at around 10^{11}–10^{13} W/cm^2, is kept low to not ionize the atom.

The initial momentum P_i of the released electron with charge e and mass m_e when appearing in the continuum, determined by Einstein's photoemission law, is $P_i = \sqrt{2m_e K_i}$, with $K_i = \hbar\omega_{XUV} - IP$ being the initial kinetic energy of the launched electron, where $\hbar\omega_{XUV}$ is the XUV central photon energy of the attosecond isolated pulse and IP is the atomic ionization threshold. The electron's motion upon release can be calculated from Newton's equations of motion in the presence of the linearly polarized along the propagating z-axis oscillating electric IR field $\boldsymbol{E}_{IR}(t)$. After the end of the laser pulse, a final modification will be imparted in the electron's momentum component parallel to the laser polarization, $\Delta p_z(\tau)$,[73,74]

$$\Delta P_z(\tau) = -eA_{IR}(\tau) = -e\int_\tau^\infty E_0(t)\cos(\omega_{IR}t + \varphi_{CE})dt, \quad (3)$$

where τ is the photoelectron's initial time of release, $A_{IR}(t)$ designates the vector potential related to the electric field $\boldsymbol{E}_{IR}(t) = E_0(t)\cos(\omega_{IR}t+\varphi_{CE})$ by $\boldsymbol{E}_{IR}(t) = -\frac{\partial A_{IR}(t)}{\partial t}$, and $E_0(t)$ is the IR's amplitude envelope of finite temporal duration meaning that only electrons being set free during the time duration of the IR pulse are streaked. Assuming the IR field vanishes for $t \to \infty$ and in the adiabatic limit $E_0\omega_{IR} \gg dE_0/dt$, Eq. (3) is written as[74]

$$\Delta P_z(\tau) = \frac{eE_0(\tau)}{\omega_{IR}}\sin(\omega_{IR}\tau + \varphi_{CE}) = \sqrt{4U_p(\tau)m_e}\sin(\omega_{IR}\tau + \varphi_{CE}), \quad (4)$$

where $U_p(\tau) = e^2E_0^2(\tau)/4m_e\omega_{IR}^2$ is the ponderomotive energy of the laser field at the time of ionization τ. Given that the initial kinetic energy is substantially greater than the ponderomotive energy in order to satisfy $K_i > 2U_p$, the released photoelectrons will experience a drift in their final kinetic energy, K_f, as a function of τ,[73]

$$K_f(\tau) = K_i + 2U_p(\tau)\cos 2\theta \sin^2(\omega_{IR}\tau + \varphi_{CE})$$
$$+ a\sqrt{8U_p(\tau)K_i}\cos\theta\sin(\omega_{IR}\tau + \varphi_{CE}), \quad (5)$$

where θ is the angle of observation measured from the z-axis and $a = \{1 - 2(U_p/K_i)\sin^2\vartheta\sin^2(\omega_{IR} + \varphi_{CE})\}^{1/2}$. Equation (5) shows that the final kinetic energy drift depends not only on the electron release time τ but also on the detection angle. For a detection angle perpendicular to the laser polarization, the kinetic energy drift will shift below K_i twice per laser period. When the detection angle is parallel to the laser polarization then the kinetic energy drift will wiggle up and down K_i as the phase of birth varies from 0 to 2π.[73] Assuming an experimental arrangement such that only photoelectrons emitted parallel to the laser polarization axis are collected ($\theta = 0°$) and that $\hbar\omega_{XUV} - I_p \gg U_p(\tau)$ (a requirement that can be relaxed since for typical working streaking IR intensities of ~10^{13} W/cm^2 the ponderomotive energy is of the order of a few tens of millielectron volt when initial kinetic energies of the released electron are in the range of several tens of electron volt), then Eq. (5) turns to

$$\Delta K(\tau) \approx \sqrt{8U_p(\tau)K_i}\sin(\omega_{IR}\tau + \varphi_{CE}) = -A_{IR}(\tau)\sqrt{\frac{2e^2}{m_e}K_i}. \quad (6)$$

Equation (6) implies that the vector potential A_{IR} of the linearly polarized streaking IR pulse is imprinted in the kinetic energy of the released electron and it can be mapped, upon varying the release time τ, into the streaking field. Hence, a streaking measurement (or spectrogram), which is composed of a series of photoelectron spectra obtained by temporally scanning the isolated attosecond pulse through the much longer femtosecond pulse, may further be used for the full characterization of the streaking laser field in the time domain.[44]

The temporal characteristics of the attosecond ionizing pulse can be derived from the photoelectron energy spectrum exploiting the effect that electron pulses released at different streaking probe times will exhibit different final spectral widths.[75,131] The ionizing pulse will reflect its temporal and time-frequency dependence (chirp) characteristics on the released electron wave packet. Since the streaking field varies over the time that photoionization takes place, the launched photoelectrons, depending on their release time t, experience different final momenta after the end of the ionizing pulse has passed. A direct consequence of this streaking effect is that the photoelectron spectrum will be generally quite different from
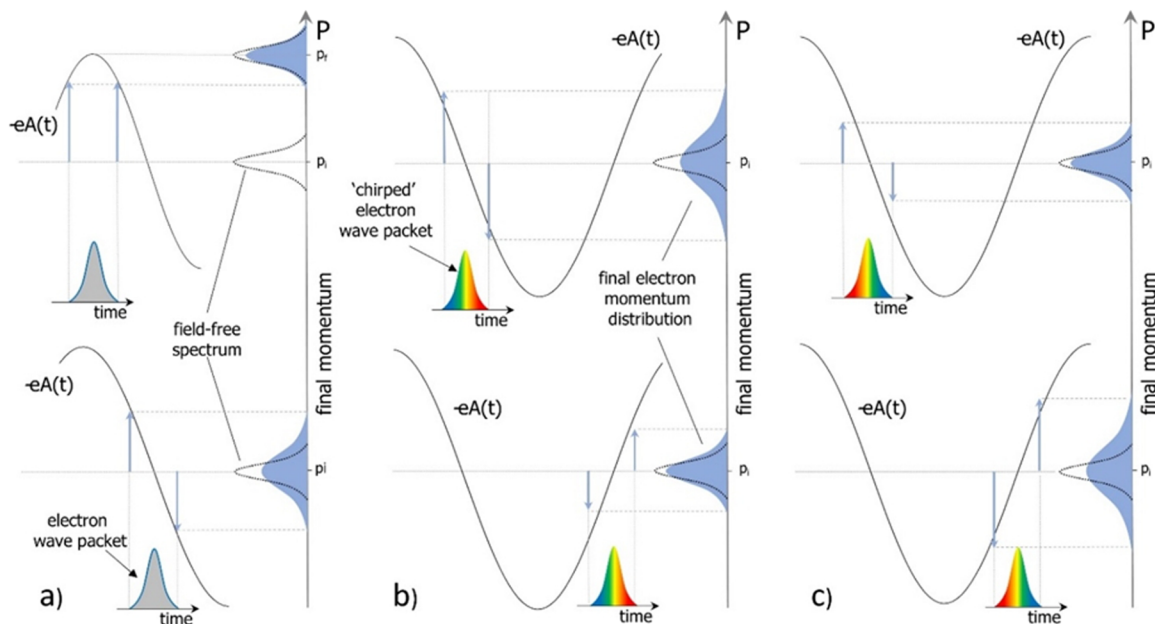
FIG. 13. (a) For unchirped (constant time-frequency evolution) electron pulses ejected at different times, a broadening of the photoelectron momentum distribution, as compared to the field-free spectrum, is exhibited whenever the release times coincide with a zero-crossing of the vector potential $A(t)$ of the streaking laser field. (b) and (c) For a positively (negatively) chirped electron pulse, the final momentum distribution is broadened (narrowed) when the electron is probed at a zero-crossing of a negative (positive) vector potential slope. Figure adapted from Ref. 132.

the streak-field-free one, i.e., when the streaking field is switched off. At a first approximation, assuming a constant vector potential within the ionizing pulse duration and an unchirped electron wave packet, an overall energy shift would be observed in the photoelectron spectrum. This is why the streaking spectrogram reflects the driver laser pulse shape. However, the vector potential does change within the ionizing pulse duration. This subtle change is being manifested as a further broadening on the photoelectron energy distribution. A broadening that is more evident when the electron release time coincides with a zero-crossing of the streaking vector potential, i.e., local electric field maximum, because in this case photoelectrons acquire opposite direction momentum shifts [Fig. 13(a)]. For a chirped attosecond pulse, the streaking effect causes a broadening or narrowing of the launched electron's final energy distribution for adjacent zero-crossings, depending on the slope sign of the streaking vector potential $-e \cdot A(t)$ probing the released photoelectron [Figs. 13(b) and 13(c)]. Assuming a positive (negative) chirp, when the electron wave packet is probed at a zero-crossing of a negative (positive) vector potential slope then the streaked photoelectron distribution will result in a broader (narrower) final electron energy distribution.

Based on the above arguments, a retrieval algorithm can be employed to fully extract the temporal characteristics of the isolated attosecond pulses. This will be discussed in more detail in Sec. III C.

2. Experimental implementation of attosecond streak camera

A typical attosecond streak camera experimental arrangement is sketched in Fig. 14. The XUV generation process is driven by a linearly polarized few-cycle IR pulse. Neon gas serves as a suitable gas target for generating the isolated attosecond XUV pulses with photon energies in the range of ~40 eV–150 eV. Both XUV and IR beams are temporally and spatially overlapped and focused on a second gas jet placed in the target area. XUV single photon ionization of ground state atoms creates a free electron wave packet with a kinetic energy K_i that is modulated by the presence of the synchronized IR few-cycle field. The final momentum of the released photoelectron depends strongly on the phase of the streaking IR electric field oscillation, i.e., the delay between the IR and XUV pulse. A positive streaking field amplitude accelerates the free electron, whereas negative amplitude leads to deceleration. Both XUV and IR pulses are considered to possess the same linear polarization, whereas the measured electron kinetic energy spectrum can be measured in various streaking detection angles with the most favorable being in parallel to the laser polarization axis. The progressive modification of the kinetic energy of the electron pulse is finally detected as a function of the time delay between the XUV and IR pulses.

C. FROG-CRAB

It was demonstrated by Refs. 80 and 133 that the attosecond streaking spectrogram allowed complete reconstruction of attosecond pulses. The technique termed FROG-CRAB is a descendent of the known FROG method[134] which is widely applied in the spectral and temporal characterization of ultrashort fs pulses. FROG-type retrieval algorithms, analyzing the measurement characteristics, can then be employed to achieve complete temporal characterization
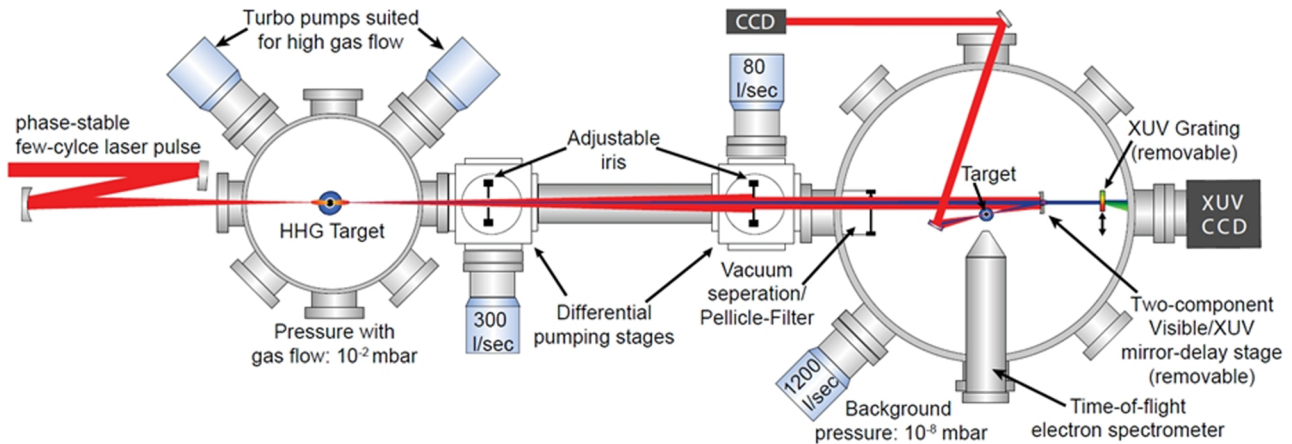
FIG. 14. Experimental setup arrangement for the attosecond streak camera technique. Figure taken from Ref. 132.

of the isolated attosecond pulses[80,121,133,135–138] and attosecond pulse trains.[139,140]

A FROG spectrogram, i.e., a 2D data spectrum set acquired as a function of time delay, is generally expressed as

$$S(\omega, \tau) = \left| \int_{-\infty}^{\infty} dt G(t) E(t - \tau) e^{i\omega t} \right|^2, \tag{7}$$

where $E(t - \tau)$ is the unknown field to be measured and $G(t)$ is the gating field. For an attosecond laser field, it was derived[80] that a similar formula with Eq. (7) can be obtained. The transition amplitude of exciting a final continuum state $|v\rangle$ of electron momentum v when only the XUV field is present, in the single active electron approximation, is expressed as[133]

$$a(v) = -i \int_{-\infty}^{\infty} dt E_{XUV}(t) \mu_{vg} e^{i(W+I_p)t}, \tag{8}$$

where $E_{XUV}(t) = E_{XUV}(t) \cdot e^{-i\omega_{XUV}t}$ is the description of the ionizing isolated attosecond XUV pulse, with $E_{XUV}(t)$ being the pulse envelope, $\mu_{vg} = \langle g|r|v \rangle$ is the dipole matrix element connecting the ground state wave function $|g\rangle$ with the continuum state wave function $|v\rangle$, $W = \frac{v^2}{2}$ is the final kinetic energy (in atomic units), and I_p is the ionization potential. If a photoelectron experiment could measure directly $\alpha(v)$ [it measures $|\alpha(v)|^2$], then $E_{XUV}(t)$ could be recovered by a Fourier transform of $\alpha(v)$. Introducing in the picture the streaking IR laser field with vector potential $A(t)$, the free electron's instantaneous momentum in the field $p(t) = v + A(t)$, including the time delay τ between the XUV-IR, in the framework of the strong field approximation and assuming that the streaking field effect on the dipole matrix is weak enough to be neglected, Eq. (8) is rewritten as[73,80,133,141]

$$a(p, \tau) = -i \int_{-\infty}^{\infty} dt E_{XUV}(t - \tau) \mu_{pg} e^{i\Theta(t-\tau)} e^{i(W+I_p)t},$$
$$\Theta(\tau) = -\int_t^{\infty} dt' \left[\left(pA(t') + \frac{1}{2} A^2(t') \right) \right]. \tag{9}$$

The resemblance of Eq. (9) with Eq. (7) becomes obvious by setting $G(t - \tau) = e^{i\Theta(t-\tau)}$, signifying that the streaking's field vector

potential modulates the emitted photoelectron wave packet as a gate function of the varying delay τ. With the use of appropriately built algorithms, complete retrieval of the attosecond pulse envelope E_{XUV} and the phase $\Theta(\tau)$ can be achieved.[80,135]

While FROG-CRAB is now a well-established method to fully characterize attosecond pulses, its application to few-femtosecond XUV pulses is not considered trivial. In particular, the associated narrower bandwidth and the subsequent loss of subcycle resolution reduce the otherwise rich level of information provided by a FROG-CRAB trace. Evolution of the ptychographic technique[137] proved its capacity to also reconstruct XUV few-femtosecond pulses down to 5 fs.[142]

1. IAP characterization with FROG-CRAB attosecond streak camera technique

The XUV broadband continuum generated with the amplitude gating method capable of supporting the isolated attosecond pulses is presented in Fig. 15(a). It was created by focusing CEP-stabilized ~5 fs NIR pulses centered at 730 nm, on a Ne gas jet. Figure 15(b) shows an experimental streaking spectrogram acquired with an XUV pulse energy centered at ~93 eV ionizing Ne gas phase atoms.[132] Both NIR and XUV copropagate to the experimental chamber of Fig. 14. Spatial separation is achieved by means of a concentric Zr foil-filter, blocking the IR beam in the center, and the inner concentric part of a focusing two-component mirror. The reflectivity of the inner mirror is centered at 93 eV with a 6.5 eV bandwidth. As shown in Fig. 15(b), the dominant contribution comes from photoelectrons stemming from the Ne 2p-cell single-photon XUV ionization centered around 71 eV, as pointed by the black solid line, while the black dashed line indicates photoelectrons coming from Ne 2s-cell ionization. In this case, the collection efficiency of the e-TOF was optimized for final energies around 70 eV. The streaking trace exhibits a low broadening, while photoelectrons are up- and down-streaked demonstrating a good interferometric stability. Employing the least squared generalized projection algorithm retrieval algorithm (LSGPA),[135] the amplitude and spectral phase of the XUV pulse can be extracted with
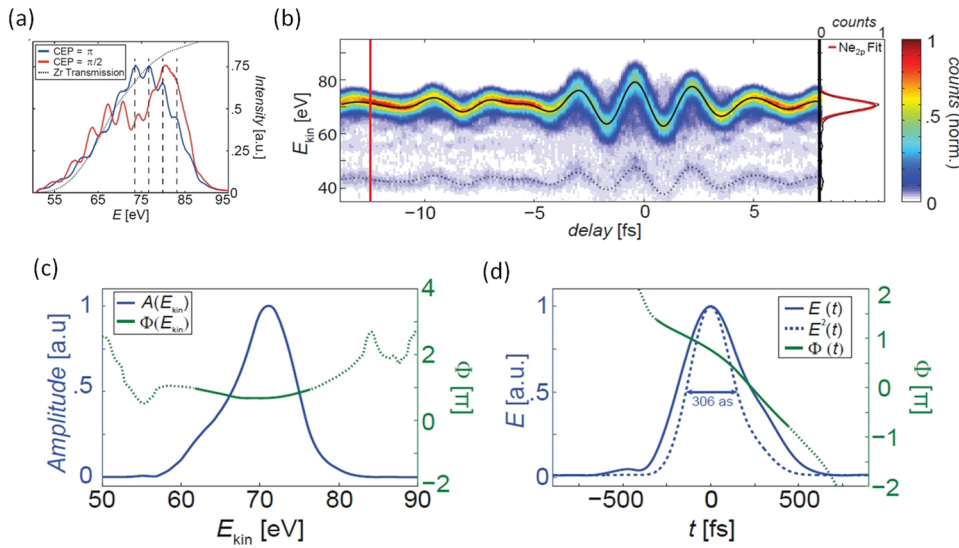
FIG. 15. (a) CEP dependence of the XUV spectra. From the superimposed dashed lines with an energy spacing of 2×1.6 eV, the central wavelength of the driving pulse can be estimated to be 729 nm. (b) Experimental streaking trace for Ne 2p-cell (solid black line) and 2s-cell (black dashed line) ionization. The right panel shows the photoelectron spectrum for the delay pointed in (b) with the red solid line. (c)–(d) LSPGA reconstructed amplitude and spectral phase. Figures taken from Ref. 132.

the results shown in Figs. 15(c) and 15(d). The inherent positive attochirp of short trajectories is partially compensated by the Zr foil filter and the XUV focusing mirror. The retrieved pulse duration is 306 as which is fairly close to the anticipated Fourier-limit of 280 as.[132]

D. Phase retrieval by omega oscillation filtering (PROOF)

An alternative to the FROG-CRAB method based on the measurement of photoelectrons spectra generated by the attosecond pulse to be characterized under the perturbation of an IR electric field is the Phase Retrieval by Omega Oscillation Filtering (PROOF) method, which is mainly appropriate for the characterization of

ultrabroadband attosecond pulses in the region of few attosecond.[81] Like the RABBIT technique, the IR perturbating dressing field is expected to be rather weak, so its action on the photoelectron spectra can be treated by means of the lowest-order perturbation theory. Both RABBIT and PROOF techniques are based on the hypothesis that only single IR photon paths are involved and contribute to the signal. It is demonstrated that the photoelectron spectrum, $I(v, \tau)$, can be expressed as the sum of three terms: $I(v, \tau) = I_o(v) + I_{\omega_L}(v, \tau) + I_{2\omega_L}(v, \tau)$ (Fig. 16), where τ is the optical delay introduced between the XUV and IR fields.

The component $I_o(v)$ signifies a term which does not depend on the delay, whereas the other two terms $I_{\omega_L}(v, \tau)$ and $I_{2\omega_L}(v, \tau)$ oscillating with frequency ω_L and $2\omega_L$, respectively, where ω_L is the IR perturbing dressing field's angular frequency. In particular, the
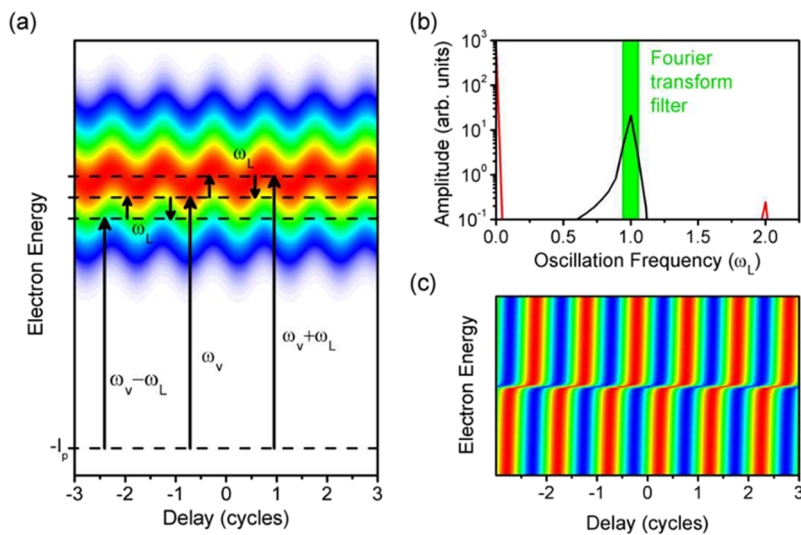
FIG. 16. Operation principle of PROOF. (a) Photoionization of electrons from an attosecond pulse to continuum states. Those continuum states separated by the laser central frequency ω_L are coupled by the perturbating IR laser, leading to the characteristic oscillation of the photoelectron signal with delay. (b) The amplitude after Fourier transforming the signal in (a). The amplitude peaks are originating from the oscillation frequencies of zero (red line), ω_L (black line), and $2\omega_L$ (red line). The ω_L component is selected by using a band-pass filter. (c) Inverse Fourier transform of the filtered ω_L component of the oscillation gives the spectrogram presented, from which the spectral phase of the attosecond pulse can be extracted. Reprinted with permission from Chini et al., Opt. Express 18, 13006 (2010). Copyright 2010 The Optical Society.

term $I_o(v)$ represents the shared probability of one (XUV) photon and two (XUV+IR) photon absorption which does not have any dependence on the delay while the terms $I_{\omega_L}(v, \tau)$ and $I_{2\omega_L}(v, \tau)$ outcome from the interferences among the different one- and two-photon channels to a given final state which are oscillated with the delay τ at the IR perturbating dressing field with laser frequency ω_L and at $2\omega_L$, respectively [Fig. 16(a)]. Since the spectral phase of the attosecond pulse is imprinted on the photoelectron wavepacket, the spectral phase of the attosecond field alterations between the interfering channels is established in the dependence of $I_{\omega_L}(v, \tau)$ on the time delay and can be extracted using a suitable mathematical method where details can be found in Ref. 81. In particular, the operation principle of the PROOF approach is summarized as follows. The atom is excited by the attosecond pulse to the continuum states in the presence of the IR dressing field. The energy of the emitted photoelectrons depicts a periodic modulation with delay as is shown in Fig. 16(a). The Fourier transform of the spectrogram in Fig. 16(a) results in the appearance of peaks at ω_L and $2\omega_L$ frequencies [Fig. 16(b)]. By applying a narrow spectrum filter, the ω_L component is filtered out from the spectrogram of Fig. 16(b) and the trace $I_{\omega_L}(v, \tau)$ is revealed [Fig. 16(c)] and used to measure the spectral phase distribution of the attosecond pulse.

PROOF was implemented in 2012 for the measurement of the isolated pulses of duration down to 67 as[143] (Fig. 17). The broadband XUV continuum radiation was generated by the Double Optical Gating (DOG) technique. The laser system used was delivering at 1 kHz rep. rate, few-cycle CEP stable IR pulses of $\approx$7 fs duration and energy 1.4 mJ/pulse. The laser pulses provided by this laser system were sent through the DOG optics and focused on a Ne-filled gas cell to produce the isolated attosecond pulses. Figure 17(a) shows a streaking trace obtained experimentally by ionizing Ne gas with XUV pulses of photon energy in the range of ~62 eV. Figures 17(b) and 17(c) show the $I_{\omega_L}(v, \tau)$ and the spectral phase of the attosecond pulse, respectively.

IV. LIMITATIONS, BOTTLENECKS, AND POTENTIAL PATHWAYS

A. 2-IVAC

Despite the large applicability of the 2-IVAC approach for the attosecond pulse characterization, as any experimental technique suffers from a series of limitations. The first one is associated with the fundamental principle of any energy not-resolved AC approach. An AC approach measures the spatiotemporal averages of pulse durations (in the case of APT provides the average duration of the
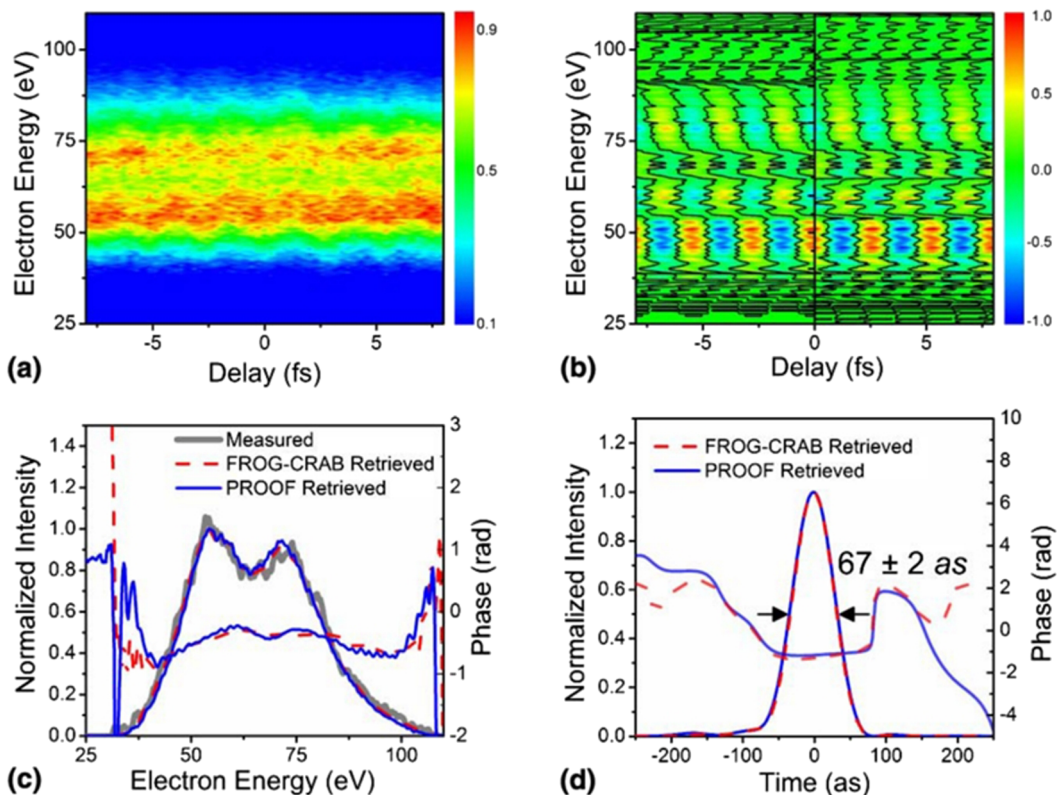
FIG. 17. XUV pulse characterization by implementing the PROOF technique. (a) Photoelectron spectrogram obtained experimentally. (b) Filtered $I_{\omega_L}(v, \tau)$ from the spectrogram in (a). (c) Photoelectron spectrum obtained experimentally (thick solid line) and retrieved spectra and spectral phases from PROOF (solid line) and FROG-CRAB (dashed line). (d) Recovered temporal profiles and spectral phases from PROOF (solid line) and FROG-CRAB (dashed line). Reprinted with permission from Zhao et al., Opt. Lett. **37**, 3891 (2012). Copyright 2012 The Optical Society.

attosecond pulses in the train) and does not allow the full pulse reconstruction. We note that the attosecond pulse duration retrieved by an AC trace recorded by measuring ions, is obtained assuming Gaussian pulses (using the relation $\tau_{XUV} = \tau_{AC}/\sqrt{2}$), an assumption which is not required in the case of XUV FROG-type measurements. Other limitations are

(a) The response of the nonlinear detector used for the pulse characterization: As any conventional AC approach, the nonlinear detector should be spectrally flat and with instantaneous response. Because the attosecond pulses are generated in different spectral regions with a bandwidth of >2 eV, to find the proper nonlinear detector is an issue far from trivial. To ensure that the properties of the nonlinear detector fulfill the requirements for attosecond pulse characterization, the proper nonlinear ionization processes need to be chosen. In order to estimate the flatness and the temporal response of the detector, the time-dependent Schrodinger equation (TDSE) needs to be solved.[84]

(b) The stability of the XUV source and both the 2-IVAC and XUV FROG techniques: A 2-IVAC measurement suffers from the intrinsic limitations that accompany any pump-probe approach that involves an interferometer (or an XUV-wave front beam splitter) as a delay line between the XUV pulses. In a 2-IVAC experiment, the XUV pulse duration is obtained by multiple shot measurements at different time delays. During these measurements, instabilities relevant to XUV-IR-laser parameters [XUV-pulse duration, XUV-intensity, carrier-envelope-phase (CEP) of the IR pulse, etc.] together with the relatively "low" peak to the background ratio provided in an ideal spatiotemporal overlap of the two XUV pulses by a 2-IVAC trace are limiting the temporal resolution of the measurement which to the best of our knowledge is in the range of 50–100 as. This value can be significantly improved by means of high rep. rate attosecond beam lines[98] or the development of single-shot XUV autocorrelator.[90,144] In addition, a robust retrieval of the phase-amplitude distributions requires high shot to shot data stability, which is rather challenging for the by nature noisy harmonic fields.

(c) The surface quality of the XUV optics: The temporal resolution of all approaches is limited by the wave front distortion upon reflection of the radiation on XUV optical elements. Achieving a surface flatness equal to a small fraction of the wavelength, assuring negligible wave front distortion is a technological challenge of, with photon energy, increasing degree of complexity and cost.

(d) The finite energy resolution of the spectrometer in XUV FROG measurements: Such measurements, in addition to the limitations mentioned above, suffer from the limited photoelectron energy resolution which is associated with resolution provided by the available electron spectrometers (which is in the range of $\Delta E/E = 1\%$, where E is the electron kinetic energy), the low PE signal, and the presence of space charge effects.

B. RABBIT

Although RABBIT has proven itself as a multipurpose method with a broad range of applications, there are several limits to its applicability in attosecond metrology. One is its capacity to only yield the average pulse shape in a given attosecond pulse train. In effect, the harmonic amplitude becomes a function of time as each harmonic field has a lower pulse duration than the fundamental pulse, with the lower orders in the XUV comb having the longest duration while the shortest belongs to the harmonics in the other end. Hence, I_{avg} in Eq. (2) becomes the average of all pulses in the attosecond pulse train. Varjú *et al.*[116] proposed a method to reconstruct pulse-to-pulse variations by performing the RABBIT measurement at different generation intensities. The method from Ref. 116 was employed in Ref. 145 to access the pulse-to-pulse variations where it was retrieved as a pulse duration which varied from 120 as in the center of the train to 140 as in the FWHM, while a pulse duration of 190 as was found at the FWTM (full-width at tenth maximum).

Measurement of average phases results in another limitation of the RABBIT approach as it was pointed out in Ref. 98 through a comparative study between 2-IVAC and RABBIT. There it was revealed as an underestimation of the APT duration when measured with the RABBIT method which was attributed to contribution effects of short and long electron trajectories in the HHG process. Overall, the findings of that first comparative study between 2-IVAC and RABBIT[98] revealed that the latter will retrieve the temporal profile of the attosecond pulse train reliably only when only one electron trajectory contributes to the wave form, particularly the short one. Elimination of the long trajectory may prove a challenging experimental requirement to relax, particularly when plateau harmonics are involved like in the case of RABBIT and APTs. Toward this direction, the use of relatively short focal length and filtering stages may be adapted to prevent the long trajectories enter the interaction region.

Another challenge in the RABBIT technique arises from the experimental necessity to keep the intensity of the dressing IR probe pulse sufficiently low in order to only act on the process as a perturbation. The validity of RABBIT will begin to break down when higher IR field intensities are involved and multiple IR photon absorption may occur, resulting in terms oscillating at higher odd and even multiples of the fundamental frequency, leading to different additional phases for a given single final state component and eventually prevent a reliable extraction of the harmonic spectral phase differences. However, such higher modulation frequencies may become useful so as to attain an unperturbed measurement for the harmonic chirp rate.[146] Furthermore, a newly developed data analysis approach termed mixed-FROG[147] is able to retrieve with greater precision the profile and pulse characteristics in a RABBIT measurement by disentangling coherent and incoherent contributions. A more recent discussion on the accuracy and precision of RABBIT measurements can be found in Ref. 148.

C. Attosecond streak camera and FROG-CRAB

Attempts on reaching shorter isolated attosecond pulse durations necessitate a broader XUV spectrum. Thus, the attosecond streak camera measurement is limited by definition of a reduced spectral resolution since the bandwidth of an IAP would be directly translated to the photoelectron energy bandwidth. The precise value of the temporal resolution of the streak camera shall be depended

on the experimental parameters such as spectrometer resolution and signal-to-noise ratio. A reasonable, though, order of magnitude estimation for the time resolution limit of a streaking measurement, indicating also the shortest pulse duration that can be measured, can be deduced by quantum mechanical time-energy uncertainty relation considerations, assuming streaking detection parallel to the laser polarization axis and electron release time near the maximum electric field strength where the vector potential is approximately linear over time. In order to resolve streaks by two distinct Δt-distanced events, the induced energy shift by the streaking field should be greater than the initial energy spread of each event,[73,131,149] which results in a fundamental quantum limitation, $\Delta t > (\hbar/E_0 p_i)^{1/2}$. It is instructive to express Δt in relation to the maximum streaked energy shift imparted on an electron with initial momentum p_i at release time T_0, $\Delta K_{max} = \frac{E_0 p_i}{\omega_{IR}}$, $\Delta t \sim (T_0/2\pi)\sqrt{\hbar\omega_{IR}/\Delta K_{max}}$. For a streaking carrier wavelength of 800 nm, a release time of ~2 fs, and typical maximum streaking shifts of 20 eV, the time dynamics of ~100 as can be potentially resolved.

Achieving better time resolution would require use of higher streaking intensities and increased ΔK_{max}, thus greater initial electron energy. An intense streaking field capable of imparting significant momentum shifts to the electron released by the IAP is required for the streaking measurement, but a more intense streaking field could ignite ATI effects to the point that may become significant generating a large amount of background electrons overlapping the useful signal. Suppression of ATI could be achieved by changing the angle (i.e., experimental geometry) of streaking detection or in the parallel detection geometry a slight ellipticity may be introduced. On the other hand, photoionization cross sections decrease with photon energy which may pose a stringent constrain to future applications of streaking-based techniques to higher photon energies and shorter pulses. To this end, observation of streaked electrons at different direction angles with respect to the laser polarization offers various advantages, for example for the perpendicular streaking detection ($\theta = 90°$), the third term of Eq. (5) is zeroed and so is the dependence of streaking shift with initial electron energy. A dependence that may become a weakness in the parallel streaking detection arrangement [$\theta = 0°$ in Eq. (5)] when electron mean release energy becomes comparable to its wave packet bandwidth. In contrast, parallel geometry offers the largest streaking effect, owing to the exact same third term of Eq. (5) which vanishes for $\theta = 90°$, along with a more direct one-to-one resemblance of the streaking spectrogram to the laser pulse shape, especially when near Fourier-transform limited pulses are in play. The parallel geometry also offers an improved streaking collection efficiency since an active detection cone as large as ±30° is reached, and it is the geometry that is mostly favored for attosecond streaking measurement setups.

It is well understood that for the streaking spectrogram, active stabilization of the carrier envelope phase φ_{CE} of the IR field is a prerequisite. The momentum shift of the released electron depends on that parameter as well. In combination with the necessity of small delay steps (in the order of few tens of attosecond) between the IAP and the streaking field so as to be able to resolve subtle changes in the attosecond time scale streaking experiments, these factors place a substantial challenge for the long-term stability of the system, in particular, because streaking measurements are performed in an electron counting regime and are intrinsically very slow (e.g., target gas

pressure, that could lead to higher count rates, is compromised by the microchannel plate detector).

A common characteristic in HHG setups is the creation of one or at cases even two, presumably weaker, satellite pulses at a distance of half-streaking laser-cycle following or preceding the main attosecond pulse. Such pulses may result in electrons being accelerated and decelerated at the same time by the streaking field which will be exhibited in more periodical oscillations in the streaking spectrogram creating spectral interference fringes in the energy domain between the different contributions. Ideally, the contribution of satellite pulses can be easily noted in the streaking spectrogram and by careful adjustment of the CEP, these may be eliminated by concentrating power to the main pulse. Else, these satellite pulses should be accounted for and through a proper fringe-resolved analysis can be integrated in the algorithm reconstruction model.[135,150]

Streaking spectrograms are formed over many laser shots, when the electron wave packet may present shot to shot uncertainties due to fluctuations of experimental parameters. To some extent, measured electron streaking spectra are an averaged result over an ensemble of wave packets. In addition, an attosecond pulse is coupled in both space and time. Under the assumption that the driving attosource is being replicated into the target medium through the produced electron pulse, then the streaking IR pulse dressing the full replica may be argued that measures the spatially averaged pulse.

Investigating the robustness of the streak camera technique and the pulse reconstruction algorithms, it relies on the identification of the effect that several key parameters (including central photon energy, bandwidth and group-delay-dispersion, and timing of the IAP and XUV-NIR delay) pose on the electron wave packet and thus in the streaking measurement itself.[151] Uncertainties in these parameters tent to be imaged as a smearing and distortions in the streaking spectrogram along the energy axis. At times, they may even result in a loss of the relative narrowing and broadening effect of the streaked wave packet when released at consecutive zero-crossings of the vector potential, affecting the recovery of the attosecond chirp. Overall, the effect of these uncertainties to some extent is reflected in overestimating the bandwidth; hence an underestimation of the pulse duration. Although each of the experimental parameters cannot be decoupled from the rest so as to determine its solely effect on the streaking and retrieval algorithms (for example, a relative time jitter will most certainly alter the relative phase), uncertainties in central photon energy, bandwidth, and group-delay dispersion at cases have been found to lead to an underestimation in the order of ~10%–15% of the original pulse, while the XUV-IR delay seems to have an even minor effect in the correct pulse reconstruction.[150]

Atomic delays, which depend on the target system, state, and photon energy, have been found to vary by several attoseconds/eV[152] and may have an impact of even 10% on the measurement accuracy of a ~100 as IAP. Disentangling the atomic response from the properties of the attosecond pulses is highly desirable, especially for sub-100 as pulses. An interesting method proposed recently reports the beneficial properties of using Rydberg wave packets to characterize attosecond UV pulses, while the technique could be readily extended to the study of shorter wavelength x-ray attosecond pulses.[153,154]

D. PROOF

The PROOF method is an extension of the RABBIT to the isolated attosecond pulses. It relies on the use of a weak dressing IR field with intensity lower that 10^{12} W/cm^2 and is based on the assumption that only paths involving a single-IR-photon absorption contribute to the signal. If the IR dressing perturbating field intensity is increased, this hypothesis becomes invalid and a systematic error can be presented in the reconstruction of the attosecond pulse. For this reason, the PROOF method suffers from the limitations described for the RABBIT approach. In addition, since PROOF relies on second order perturbation theory and deals with the metrology of pulse in the few-attosecond time scale, any participation streaking in the photoelectron signal, may introduce substantial errors on the retrieval of the spectral phase distribution of the IAP. A promising alternative to PROOF as well as to FROG-CRAB methods on retrieving spectral phases with neural networks has been recently developed, with potential application to the characterization of x-ray FEL pulses.[155]

V. CHALLENGES AND FUTURE DIRECTIONS

A. High photon flux attosecond pulses in the XUV range

Noble gas atoms driven by high power infrared (IR) laser pulses have been routinely employed over the years for the production of subfemtosecond pulses in the 20–100 eV XUV photon energy regime, yielding photon fluxes ranging from 10^7 to 10^{11} photons/pulse.[31–40] The latest technological advance toward an XUV high photon flux attosecond pulsed source is the newly constructed ≈18 m long (HHG) beam line based on loose focusing geometry (driving laser focused using 9 m focal length) and a double gas jet target arrangement of the Attosecond Science and Technology Laboratory of the Foundation of Research and Technology (FORTH).[39] By operating the beam line at optimal driving intensities and xenon gas pressure/two-jet-distance, enabling optimal phase matching, an XUV energy per pulse of 230 μJ has been demonstrated in the spectral region 20–30 eV. The corresponding photon flux of 0.6×10^{14} photons/pulse is competitive with FEL photon fluxes in this spectral region. Although not measured yet, it is expected from previous measurements that the harmonics form an APT. An estimated envelope width of 10 fs duration and a measured XUV focal spot size of 2 μm[89,90] result in an achieved focused intensity of ~7×10^{15} W/cm^2, a value that by using high reflectivity XUV optics can be increased to 10^{17} W/cm^2. These high XUV intensities are evidenced by witnessing multiply charged argon atoms (observed charge states up to Ar^{4+}) produced by multi-XUV-photon ionization processes. Combining polarization gating approaches[100,101] with CEP tagging schemes[156] it is estimated that such a beam line can deliver the isolated attosecond pulses with power in the experimental target area in the range of ~few GW/pulse. Such unprecedented high power, for the current table-top HHG arrangements, will open up unique and exciting pathways toward XUV-pump-XUV-probe electronic studies in atoms, molecules, and solids while it will pave the way for exploiting new nonlinear schemes for attosecond pulse characterization.

The measurement of the temporal duration of an XUV pulse under investigation may be down limited by the ionization potential of the target atom (A) which inherently sets an upper limit to the harmonic order q that would be permitted to be included in the superposition. This limitation can be surpassed by exploiting alternative two-XUV-photon ionization schemes, such as the nonresonant direct double ionization (DDI), sequential double ionization (SDI), and above threshold ionization (ATI) (Fig. 18),[34,39,40,47,58,157–159] where the corresponding products of ionization, ions or electrons are collected by means of ion-TOF mass or time-resolved photoelectron, spectroscopy.

The ATI scheme offers the advantage of continuously extending the 2nd order AC technique to shorter wavelengths, thus higher photon energies. Given that the ATI photons reach a structureless continuum (i.e., there are no autoionizing bound atomic states present), then this advantage becomes the only constraint of the method, as the cross section decreases rapidly with photon energy [$\propto (\hbar \omega)^{-6}$[160]].

The two-photon-ATI scheme produces singly charged ions and electrons with discrete energies $PE_m^{ATI} = \hbar \omega_m - IP_1$, where $m = q_{min} + q_{max} + n$ with $n = 1 - N, \ldots, N - 1$; q_{min} and q_{max} are the minimum and maximum harmonic orders spanning the XUV comb, N is the number of harmonics in the superposition and IP_1 is the first atomic ionization threshold. Photoelectron spectroscopy is required to energy-resolve the different groups of electron energies.
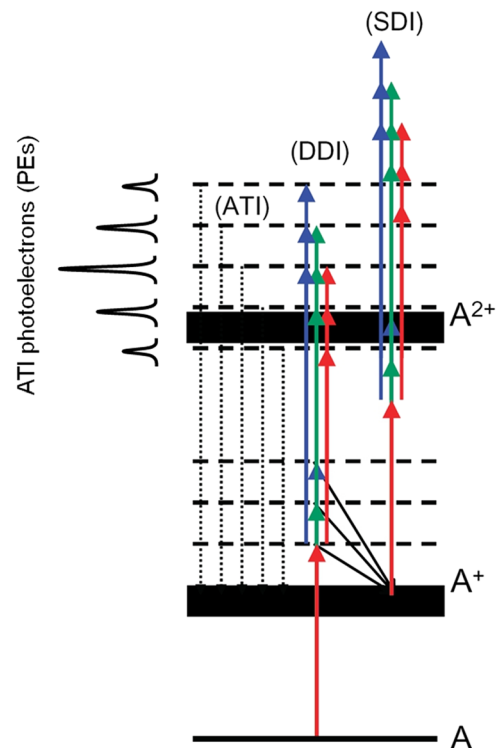
FIG. 18. Ionization scheme showing the ATI, DDI, and SDI processes of an atom A. ATI leads to the generation of a singly charged ion and photoelectrons (PEs) with energies depending on the energies of the photons involved in the ionization process. DDI and SDI generate doubly charged ions and PEs with energies depending on the energies of the photons involved in the ionization process. These processes allow the extension of the AC method to higher photon energies.

The DDI and SDI schemes also allow an extension of the second-order AC method to shorter wavelengths, but with the additional constraint that photon energies lie in the region $IP_1 < \hbar\omega_q < IP_2 - IP_1$, with IP_2 being the second atomic ionization potential. Here, both ion mass spectrometry collecting doubly charged ions and PE spectroscopy can be employed. In this photon energy region, there are several ionization pathways that can contribute to the products of ionization, such as single-photon, two-photon DDI (TPDDI), and three-photon SDI (ThPSDI), each with its own ionization rate. The single-photon ionization process is not taken into consideration because it does not contain any temporal pulse characteristic information. The TPDDI and ThPSDI mechanisms lead to the formation of doubly charged ions (A^{2+}) and electrons with energies $0 < PE_{ch}^{DDI} < \hbar\omega_{ch} - IP_2$ and $PE_{ch}^{ThPSDI} = \hbar\omega_{ch} - (IP_2 - IP_1)$, respectively. Since there is no direct way of discriminating the coexisting contribution of both schemes in the recorded signal in the ionization process, the temporal evolution of the system can be evaluated at different intensities using rate equations.[161,162] Nonetheless, results of previous studies in He, Ar, and Kr[40,57,58,66,157,158,161,162] render possible a rough estimation of the intensity regions where the second-order AC method can be applied for attosecond pulse train characterization through DDI or SDI excitation schemes. According to previous studies in the He atom,[162] for XUV intensities well below the SDI saturation intensity of the atom ($I_{XUV} < 10^{13}$ W/cm^2), the TPDDI and ThPSDI rates are expressed as $W_2^{DDI} = \sigma_{DDI}^{(2)} I_{XUV}^{(q)} I_{XUV}^{(p)} / (\hbar^2 \omega_q \omega_p)$ and $W_3^{ThPSDI} = \left[\sigma^{(1)} I_{XUV}^{(q)} / \hbar\omega_q \right]\left[\sigma_{TPII}^{(2)} I_{XUV}^{(q)} I_{XUV}^{(p)} / (\hbar^2 \omega_q \omega_p) \right]$, respectively; σ_{TPII} denotes the two-photon ionization cross section of the ion. In that case, DDI becomes the dominant process that could be used for attosecond pulse characterization. When employed intensities are far above the SDI saturation intensity of the atom ($I_{XUV} > 3 \times 10^{15}$ W/cm^2), the ThPSDI rate is expressed as the product of the ionic saturated ground state population times the ionic two-photon ionization rate, i.e., $W_3^{ThPSDI} = \left[Y_1^{(q)} / N \right]\left[\sigma_{TPII}^{(2)} I_{XUV}^{(q)} I_{XUV}^{(p)} / (\hbar^2 \omega_q \omega_p) \right]$, which effectively is a second-order process. Then, the SDI process dominates and is favored to be used for attosecond pulse duration measurements, namely, through its second step, i.e., the two-photon ionization of the ion, with the atomic population being depleted.

Besides the usefulness of the above schemes on characterizing intense attosecond pulses in different XUV spectral regions, the relatively low peak to background ratio provided by the 2-IVAC technique is limiting the temporal resolution of the measurement. Hence, high dynamic range correlation approaches which are commonly used in the Ti:sa laser fs metrology are missing from the toolbox of the attosecond pulse metrology. Such approaches are now feasible to be implemented in the XUV spectral range using high nonlinear processes induced by XUV pulses with power in the GWatt range.

B. Attosecond pulses in the water-window regime

Hitherto, most attosecond science studies have been confined at <125 eV photon energies where predominantly valence electron related dynamics can be investigated. Scaling attosecond pulses, and their characterization, to the soft x-ray regime would allow ionization of core level electrons and give access to a number of fundamental processes and triggering events, including key elements

of biological systems. Longer driver wavelengths, i.e., mid-IR, have proved to be beneficial for HHG overcoming plasma-induced dispersion related constraints and could lead to the production of attosecond pulses with photon energies up to the kilo-electron-volt range.[163,164] Recently, an elaborate water-window beam line at the Institute of Photonic Sciences (ICFO)[165,166] has provided exciting new results. They report on a cross correlation streaking measurement, evidencing an ultrabroadband soft x-ray isolated attosecond pulse, produced by means of HHG in neon gas, using a 2-cycle (~12 fs) Ti:sa seeded CEP-stabilized laser source of carrier wavelength at 1.85 μm, 0.4 mJ/pulse at the 1 kHz repetition rate. Even if a direct application of streaking retrieval algorithms was not possible, simulations based on FROG-CRAB or LSGPA algorithms yield an upper time limit for its temporal duration of ~320 as.[166] Further efforts are required, and several are currently under way to overcome experimental difficulties and circumvent retrieval algorithm related constraints, so as to produce and fully characterize high brilliance coherent ultrabroad band water-window attosecond pulses.[167]

C. Novel attosecond pulse sources at ELI-ALPS

Of particular importance here are the perspectives opened these days by the development of high average-, high peak-power, CEP stabilized few cycle laser systems acting as driving laser sources of attosecond beam-lines similar to the one of FORTH-IESL.[39] One such example is the so called SYLOS laser system recently installed at the Extreme Light Infrastructure Attosecond Light Source (ELI-ALPS).[168] With such driving sources, 10 GW (or higher) class, attosecond sources can be operated at 1 kHz repetition rates which in combination with advance devices, such as Reaction Microscopes, allow for electron-electron, electron-ion, and ion-ion coincidence experiments. XUV-pump-XUV-prove coincidence measurements with attosecond temporal resolution will allow kinematically complete or close to complete experiments in a very broad spectrum of forefront topics in ultrafast Atomic, Molecular and Optical (AMO) physics, chemistry, and biology. It is expected that in the next decade such experimental opportunities will be available at several laboratories worldwide, starting from large Research Infrastructures and going over to Research Institutions and Universities, beneficial for research and education.

VI. CONCLUSIONS

The harvest of a two decades long trip through the intricacies of attosecond pulse metrology is abundant in groundbreaking science that has created a rich arsenal of novel methods and technologies. Together with the advancement in laser technology and laser based coherent XUV beam-lines, attosecond pulse metrology enjoys a continuous improvement, circumventing all the bottlenecks arising when entering the XUV spectral range. This progress has enabled increased accuracy, reliability, robustness, and more complete information on the parameters underlying the deduction of the temporal shape of attosecond pulses. Temporal resolution reaches the order of 1 as and allows the metrology of ten attosecond scale pulses and characteristic times of ultrafast phenomena. Novel methods, increased stability, and resolution permit the extraction of detailed parameters necessary for the reconstruction of attosecond pulse profiles. Despite the massive advancement, there is still a number of limitations in all the developed methods and the lack

of rigorous comparative studies between the different methods toward the establishment of norms. Thus, attosecond pulse metrology remains an open research field with notable potential for innovative initiatives, upgrades, and vanguard science. In this article, the most frequently used attosecond pulse metrology methods and technologies have been reviewed highlighting their capacity and limitations that signalize future progressions.[169] Advancement in laser technology, in particular toward high average-, high peak-power driving laser systems, will play pivotal role in attosecond science in the coming years.

ACKNOWLEDGMENTS

REFERENCES

[1] T. Maiman, "Stimulated optical radiation in Ruby," Nature **187**, 493 (1960).

[2] F. J. McClung and R. W. Hellwarth, "Giant optical pulsations from Ruby," J. Appl. Phys. **33**, 828 (1962).

[3] A. J. DeMaria, D. A. Stetser, and H. Heynau, "Self mode-locking of lasers with saturable absorbers," Appl. Phys. Lett. **8**, 174 (1966).

[4] P. F. Moulton, "Spectroscopic and laser characteristics of Ti:Al$_2$O$_3$," J. Opt. Soc. Am. B **3**, 125 (1986).

[5] R. L. Fork, C. H. Brito Cruz, P. C. Becker, and C. V. Shank, "Compression of optical pulses to six femtoseconds by using cubic phase compensation," Opt. Lett. **12**, 483 (1987).

[6] D. Strickland and G. Mourou, "Compression of amplified chirped optical pulses," Opt. Commun. **56**, 219 (1985).

[7] D. Strickland, "Nobel Lecture: Generating high-intensity ultrashort optical pulses," Rev. Mod. Phys. **91**, 030502 (2019).

[8] A. H. Zewail, "Femtochemistry: Atomic-scale dynamics of the chemical bond," J. Phys. Chem. A **104**, 5660–5694 (2000).

[9] K. J. Schafer, B. Yang, L. I. DiMauro, and K. C. Kulander, "Above threshold ionization beyond the high harmonic cutoff," Phys. Rev. Lett. **70**, 1599 (1993).

[10] P. B. Corkum, "Plasma perspective on strong-field multiphoton ionization," Phys. Rev. Lett. **71**, 1994 (1993).

[11] M. Lewenstein, Ph. Balcou, M. Yu. Ivanov, A. L'Huillier, and P. B. Corkum, "Theory of high harmonic generation by low-frequency laser fields," Phys. Rev. A **49**, 2117 (1994).

[12] A. McPherson, G. Gibson, H. Jara, U. Johann, T. S. Luk, I. A. McIntyre, K. Boyer, and C. K. Rhodes, "Studies of multiphoton production of vacuum-ultraviolet radiation in the rare gases," J. Opt. Soc. Am. B **4**, 595 (1987).

[13] M. Ferray, A. L'Huillier, X. F. Li, L. A. Lomprk, G. Mainfray, and C. Manus, "Multiple-harmonic conversion of 1064 nm radiation in rare gases," J. Phys. B: At., Mol. Opt. Phys. **21**, L31 (1988).

[14] X. F. Li, A. L'Huillier, M. Ferray, L. A. Lompre, and G. Mainfray, "Multiple-harmonic generation in rare gases at high laser intensity," Phys. Rev. A **39**, 5751 (1989).

[15] T. W. Hänsch, "A proposed sub-femtosecond pulse synthesizer using separate phase-locked laser oscillators," Opt. Commun. **80**, 71 (1990).

[16] Gy. Farkas and Cs. Tóth, "Proposal for attosecond light pulse generation using laser induced multiple-harmonic conversion processes in rare gases," Phys. Lett. A **168**, 447 (1992).

[17] S. E. Harris, J. J. Macklin, and T. W. Hänsch, "Atomic scale temporal structure inherent to high-order harmonic generation," Opt. Commun. **100**, 487 (1993).

[18] P. B. Corkum and F. Krausz, "Attosecond science," Nat. Phys. **3**, 381 (2007).

[19] F. Krausz and M. Ivanov, "Attosecond physics," Rev. Mod. Phys. **81**, 163 (2009).

[20] A. Acín, I. Bloch, H. Buhrman, T. Calarco, C. Eichler, J. Eisert, D. Esteve, N. Gisin, S. J. Glaser, F. Jelezko, S. Kuhr, M. Lewenstein, M. F. Riedel, P. O. Schmidt, R. Thew, A. Wallraff, I. Walmsley, and F. K. Wilhelm, "The quantum technologies roadmap: A European community view," New J. Phys. **20**, 080201 (2018).

[21] I. A. Gonoskov, N. Tsatrafyllis, I. K. Kominis, and P. Tzallas, "Quantum optical signatures in strong-field laser physics: Infrared photon counting in high-order-harmonic generation," Sci. Rep. **6**, 32821 (2016).

[22] N. Tsatrafyllis, I. K. Kominis, I. A. Gonoskov, and P. Tzallas, "High-order harmonics measured by the photon statistics of the infrared driving-field exiting the atomic medium," Nat. Commun. **8**, 15170 (2017).

[23] N. Tsatrafyllis, S. Kuhn, M. Dumergue, P. Foldi, S. Kahaly, E. Cormier, I. A. Gonoskov, B. Kiss, K. Varju, S. Varro, and P. Tzallas, "Quantum optical signatures in a strong laser pulse after interaction with semiconductors," Phys. Rev. Lett. **122**, 193602 (2019).

[24] A. Wirth, M. T. Hassan, I. Grguras, J. Gagnon, A. Moulet, T. T. Luu, S. Pabst, R. Santra, Z. A. Alahmed, A. M. Azzeer, V. S. Yakovlev, V. Pervak, F. Krausz, and E. Goulielmakis, "Synthesized light transients," Science **334**, 195 (2011).

[25] S. Chatziathanasiou, S. Kahaly, E. Skantzakis, G. Sansone, R. Lopez-Martens, S. Haessler, K. Varju, G. Tsakiris, D. Charalambidis, and P. Tzallas, "Generation of attosecond light pulses from gas and solid state media," Photonics **4**, 26 (2017).

[26] C. M. Heyl, H. Coudert-Alteirac, M. Miranda, M. Louisy, K. Kovacs, V. Tosa, E. Balogh, K. Varjú, A. L'Huillier, A. Couairon, and C. L. Arnold, "Scale-invariant nonlinear optics in gases," Optica **3**, 75 (2016).

[27] F. Silva, D. R. Austin, A. Thai, M. Baudisch, M. Hemmer, D. Faccio, A. Couairon, and J. Biegert, "Multi-octave supercontinuum generation from mid-infrared filamentation in a bulk crystal," Nat. Commun. **3**, 807 (2012).

[28] F. Silva, S. M. Teichmann, S. L. Cousin, M. Hemmer, and J. Biegert, "Spatiotemporal isolation of attosecond soft X-ray pulses in the water window," Nat. Commun. **6**, 6611 (2015).

[29] T. Popmintchev, M. C. Chen, D. Popmintchev, P. Arpin, S. Brown, S. Ališauskas, G. Andriukaitis, T. Balčiunas, O. D. Mücke, A. Pugzlys, A. Baltuška, B. Shim, S. E. Schrauth, A. Gaeta, C. Hernández-García, L. Plaja, A. Becker, A. Jaron-Becker, M. M. Murnane, and H. C. Kapteyn, "Bright coherent ultra-high harmonics in the keV x-ray regime from mid-infrared femtosecond lasers," Science **336**, 1287 (2012).

[30] T. Gaumnitz, A. Jain, Y. Pertot, M. Huppert, I. Jordan, F. Ardana-Lamas, and H. J. Wörner, "Streaking of 43-attosecond soft-X-ray pulses generated by a passively CEP-stable mid-infrared driver," Opt. Express **25**, 27506 (2017).

[31] E. Constant, D. Garzella, P. Breger, E. Mével, C. Dorrer, C. Le Blanc, F. Salin, and P. Agostini, "Optimizing high harmonic generation in absorbing gases: Model and experiment," Phys. Rev. Lett. **82**, 1668 (1999).

[32] J.-F. Hergott, M. Kovacev, H. Merdji, C. Hubert, Y. Mairesse, E. Jean, P. Breger, P. Agostini, B. Carré, and P. Salières, "Extreme-ultraviolet high-order harmonic pulses in the microjoule range," Phys. Rev. A **66**, 021801 (2002).

[33] E. Skantzakis, P. Tzallas, J. Kruse, C. Kalpouzos, and D. Charalambidis, "Coherent continuum extreme ultraviolet radiation in the sub-100-nJ range generated by a high-power many-cycle laser field," Opt. Lett. **34**, 1732 (2009).

[34] P. Tzallas, E. Skantzakis, L. A. A. Nikolopoulos, G. D. Tsakiris, and D. Charalambidis, "Extreme-ultraviolet pump–probe studies of one-femtosecond-scale electron dynamics," Nat. Phys. **7**, 781 (2011).

[35] G. Sansone, L. Poletto, and M. Nisoli, "High-energy attosecond light sources," Nat. Photonics **5**, 655 (2011).

[36] E. J. Takahashi, P. Lan, O. D. Mucke, Y. Nabekawa, and K. Midorikawa, "Attosecond nonlinear optics using gigawatt-scale isolated attosecond pulses," Nat. Commun. **4**, 2691 (2013).

[37]Y. Wu, E. Cunningham, H. Zang, J. Li, M. Chini, X. Wang, Y. Wang, K. Zhao, and Z. Chang, "Generation of high-flux attosecond extreme ultraviolet continuum with a 10 TW laser," Appl. Phys. Lett. **102**, 201104 (2013).

[38]E. J. Takahashi, P. Lan, O. D. Mucke, Y. Nabekawa, and K. Midorikawa, "Infrared two-color multicycle laser field synthesis for generating an intense attosecond pulse," Phys. Rev. Lett. **104**, 233901 (2010).

[39]A. Nayak, I. Orfanos, I. Makos, M. Dumergue, S. Kühn, E. Skantzakis, B. Bodi, K. Varju, C. Kalpouzos, H. I. B. Banks, A. Emmanouilidou, D. Charalambidis, and P. Tzallas, "Multiple ionization of argon via multi-XUV-photon absorption induced by 20-GW high-order harmonic laser pulses," Phys. Rev. A **98**, 023426 (2018).

[40]K. Midorikawa, Y. Nabekawa, and A. Suda, "XUV multiphoton processes with intense high-order harmonics," Prog. Quantum Electron. **32**, 43 (2008).

[41]S. M. Teichmann, F. Silva, S. L. Cousin, M. Hemmer, and J. Biegert, "0.5-keV soft X-ray attosecond continua," Nat. Commun. **7**, 11493 (2016).

[42]B. Schütte, P. Weber, K. Kovács, E. Balogh, B. Major, V. Tosa, S. Han, M. Vrakking, K. Varjú, and A. Rouzée, "Bright attosecond pulse generation under transient phase-matching in two-colour high-order harmonic generation," Opt. Express **23**, 33947 (2015).

[43]G. G. Paulus, F. Grasbon, H. Walther, P. Villoresi, M. Nisoli, S. Stagira, E. Priori, and S. de Silvestri, "Absolute-phase phenomena in photoionization with few-cycle laser pulses," Nature **414**, 182 (2001).

[44]E. Goulielmakis, V. S. Yakovlev, A. L. Cavalieri, M. Uiberacker, V. Pervak, A. Apolonski, R. Kienberger, U. Kleineberg, and F. Krausz, "Attosecond control and measurement: Lightwave electronics," Science **317**, 769 (2007).

[45]F. Frank, C. Arrell, T. Witting, W. A. Okell, J. McKenna, J. S. Robinson, C. A. Haworth, D. Austin, H. Teng, I. A. Walmsley, J. P. Marangos, and J. W. G. Tisch, "Technology for attosecond science," Rev. Sci. Instrum. **83**, 071101 (2012).

[46]F. Frassetto, A. Trabattoni, S. Anumula, G. Sansone, F. Calegari, M. Nisoli, and L. Poletto, "High-throughput beamline for attosecond pulses based on toroidal mirrors with microfocusing capabilities," Rev. Sci. Instrum. **85**, 103115 (2014).

[47]B. Manschwetus, L. Rading, F. Campi, S. Maclot, H. Coudert-Alteirac, J. Lahl, H. Wikmark, P. Rudawski, C. M. Heyl, B. Farkas, T. Mohamed, A. L'huillier, and P. Johnsson, "Two-photon double ionization of neon using an intense attosecond pulse train," Phys. Rev. A **93**, 061402 (2016).

[48]S. Kühn, M. Dumergue, S. Kahaly, S. Mondal, M. Füle, T. Csizmadia, B. Farkas, B. Major, Z. Várallyay, E. Cormier, M. Kalashnikov, F. Calegari, M. Devetta, F. Frassetto, E. Månsson, L. Poletto, S. Stagira, C. Vozzi, M. Nisoli, P. Rudawski, S. Maclot, F. Campi, H. Wikmark, C. L. Arnold, C. M. Heyl, P. Johnsson, A. L'Huillier, R. Lopez-Martens, S. Haessler, M. Bocoum, F. Boehle, A. Vernier, G. Iaquaniello, E. Skantzakis, N. Papadakis, C. Kalpouzos, P. Tzallas, F. Lépine, D. Charalambidis, K. Varjú, K. Osvay, and G. Sansone, "The ELI-ALPS facility," J. Phys. B: At., Mol. Opt. Phys. **50**, 132002 (2017).

[49]N. Dudovich, O. Smirnova, J. Levesque, Y. Mairesse, M. Yu. Ivanov, D. M. Villeneuve, and P. B. Corkum, "Measuring and controlling the birth of attosecond XUV pulses," Nat. Phys. **2**, 781 (2006).

[50]K. T. Kim, C. Zhang, A. D. Shiner, B. E. Schmidt, F. Légaré, D. M. Villeneuve, and P. B. Corkum, "Petahertz optical oscilloscope," Nat. Photonics **7**, 958 (2013).

[51]Y. Mairesse, O. Gobert, P. Breger, H. Merdji, P. Meynadier, P. Monchicourt, M. Perdrix, P. Salières, and B. Carré, "High harmonic XUV spectral phase interferometry for direct electric-field reconstruction," Phys. Rev. Lett. **94**, 173903 (2005).

[52]E. Cormier, I. A. Walmsley, E. M. Kosik, A. S. Wyatt, L. Corner, and L. F. DiMauro, "Self-referencing, spectrally, or spatially encoded spectral interferometry for the complete characterization of attosecond electromagnetic pulses," Phys. Rev. Lett. **94**, 033905 (2005).

[53]O. Pedatzur, A. Trabattoni, B. Leshem, H. Shalmoni, M. C. Castrovilli, M. Galli, M. Lucchini, E. Månsson, F. Frassetto, L. Poletto, B. Nadler, O. Raz, M. Nisoli, F. Calegari, D. Oron, and N. Dudovich, "Double-blind holography of attosecond pulses," Nat. Photonics **13**, 91 (2019).

[54]P. Tzallas, D. Charalambidis, N. A. Papadogiannis, K. Witte, and G. D. Tsakiris, "Direct observation of attosecond light bunching," Nature **426**, 267 (2003).

[55]Y. Nabekawa, T. Shimizu, T. Okino, K. Furusawa, H. Hasegawa, K. Yamanouchi, and K. Midorikawa, "Conclusive evidence of an attosecond pulse train observed with the mode-resolved autocorrelation technique," Phys. Rev. Lett. **96**, 083901 (2006).

[56]P. Tzallas, D. Charalambidis, N. A. Papadogiannis, K. Witte, and G. D. Tsakiris, "Second-order autocorrelation measurements of attosecond XUV pulse trains," J. Mod. Opt. **52**, 321 (2005).

[57]T. Sekikawa, A. Kosuge, T. Kanai, and S. Watanabe, "Nonlinear optics in the extreme ultraviolet," Nature **432**, 605 (2004).

[58]A. Kosuge, T. Sekikawa, X. Zhou, T. Kanai, S. Adachi, and S. Watanabe, "Frequency-resolved optical gating of isolated attosecond pulses in the extreme ultraviolet," Phys. Rev. Lett. **97**, 263901 (2006).

[59]Y. Nomura, R. Hörlein, P. Tzallas, B. Dromey, S. Rykovanov, Z. Major, J. Osterhoff, S. Karsch, L. Veisz, M. Zepf, D. Charalambidis, F. Krausz, and G. D. Tsakiris, "Attosecond phase locking of harmonics emitted from laser-produced plasmas," Nat. Phys. **5**, 124 (2009).

[60]P. A. Carpeggiani, P. Tzallas, A. Palacios, D. Gray, F. Martín, and D. Charalambidis, "Disclosing intrinsic molecular dynamics on the 1-fs scale through extreme-ultraviolet pump-probe measurements," Phys. Rev. A **89**, 023420 (2014).

[61]T. Okino, Y. Furukawa, Y. Nabekawa, S. Miyabe, A. Amani Eilanlou, E. J. Takahashi, K. Yamanouchi, and K. Midorikawa, "Direct observation of an attosecond electron wave packet in a nitrogen molecule," Sci. Adv. **1**, e1500356 (2015).

[62]Y. Nabekawa, Y. Furukawa, T. Okino, A. A. Eilanlou, E. J. Takahashi, K. Yamanouchi, and K. Midorikawa, "Settling time of a vibrational wavepacket in ionization," Nat. Commun. **6**, 8197 (2015).

[63]E. Skantzakis, P. Tzallas, J. E. Kruse, C. Kalpouzos, O. Faucher, G. D. Tsakiris, and D. Charalambidis, "Tracking autoionizing-wave-packet dynamics at the 1-fs temporal scale," Phys. Rev. Lett. **105**, 043902 (2010).

[64]Y. Kobayashi, T. Sekikawa, Y. Nabekawa, and S. Watanabe, "27-fs extreme ultraviolet pulse generation by high-order harmonics," Opt. Lett. **23**, 64 (1998).

[65]K. Furusawa, T. Okino, T. Shimizu, H. Hasegawa, Y. Nabekawa, K. Yamanouchi, and K. Midorikawa, "Photoelectron spectroscopy of two-photon ionisation of rare-gas atoms by multiple high order harmonics," Appl. Phys. B **83**, 203 (2006).

[66]E. P. Benis, D. Charalambidis, T. N. Kitsopoulos, G. D. Tsakiris, and P. Tzallas, "Two-photon double ionization of rare gases by a superposition of harmonics," Phys. Rev. A **74**, 051402(R) (2006).

[67]E. Goulielmakis, G. Nersisyan, N. A. Papadogiannis, D. Charalambidis, G. D. Tsakiris, and K. Witte, "A dispersionless Michelson interferometer for the characterization of attosecond pulses," Appl. Phys. B **74**, 197 (2002).

[68]N. A. Papadogiannis, G. Nersisyan, E. Goulielmakis, T. P. Rakitzis, E. Hertz, D. Charalambidis, G. D. Tsakiris, and K. Witte, "Temporal characterization of short-pulse third-harmonic generation in an atomic gas by a transmission-grating Michelson interferometer," Opt. Lett. **27**, 1561 (2002).

[69]E. Papalazarou, M. Kovačev, P. Tzallas, E. P. Benis, C. Kalpouzos, G. D. Tsakiris, and D. Charalambidis, "Spectral phase distribution retrieval through coherent control of harmonic generation," Phys. Rev. Lett. **96**, 163901 (2006).

[70]P. Tzallas, E. Skantzakis, E. P. Benis, C. Kalpouzos, G. D. Tsakiris, and D. Charalambidis, "Full temporal reconstruction of a lower order harmonic superposition," New J. Phys. **9**, 232 (2007).

[71]P. M. Paul, E. S. Toma, P. Breger, G. Mullot, F. Auge, P. Balcou, H. G. Muller, and P. Agostini, "Observation of a train of attosecond pulses from high harmonic generation," Science **292**, 1689 (2001).

[72]M. Hentschel, R. Kienberger, C. Spielmann, G. A. Reider, N. Milosevic, T. Brabec, P. B. Corkum, U. Heinzmann, M. Drescher, and F. Krausz, "Attosecond metrology," Nature **414**, 509 (2001).

[73]J. Itatani, F. Quéré, G. L. Yudin, M. Y. Ivanov, F. Krausz, and P. B. Corkum, "Attosecond streak camera," Phys. Rev. Lett. **88**, 173903 (2002).

[74]M. Drescher, M. Hentschel, R. Kienberger, G. Tempea, C. Spielmann, G. A. Reider, P. B. Corkum, and F. Krausz, "X-ray pulses approaching the attosecond frontier," Science **291**, 1923 (2001).

[75]E. Goulielmakis, M. Uiberacker, R. Kienberger, A. Baltuska, V. Yakovlev, A. Scrinzi, T. Westerwalbesloh, U. Kleineberg, U. Heinzmann, M. Drescher, and F. Krausz, "Direct measurement of light waves," Science **305**, 1267 (2004).

[76] R. Kienberger, M. Hentschel, M. Uiberacker, Ch. Spielmann, M. Kitzler, A. Scrinzi, M. Wieland, T. Westerwalbesloh, U. Kleineberg, U. Heinzmann, M. Drescher, and F. Krausz, "Steering attosecond electron wave packets with light," Science 297, 1144 (2002).

[77] M. Uiberacker, T. Uphues, M. Schultze, A. J. Verhoef, V. Yakovlev, M. F. Kling, J. Rauschenberger, N. M. Kabachnik, H. Schröder, M. Lezius, K. L. Kompa, H.-G. Muller, M. J. J. Vrakking, S. Hendel, U. Kleineberg, U. Heinzmann, M. Drescher, and F. Krausz, "Attosecond real-time observation of electron tunnelling in atoms," Nature 446, 627 (2007).

[78] M. Reduzzi, P. Carpeggiani, S. Kühn, F. Calegari, M. Nisoli, S. Stagira, C. Vozzi, P. Dombi, S. Kahaly, P. Tzallas, D. Charalambidis, K. Varju, K. Osvay, and G. Sansone, "Advances in high-order harmonic generation sources for time-resolved investigations," J. Electron Spectrosc. Relat. Phenom. 204, 257 (2015).

[79] A. L. Cavalieri, N. Müller, T. Uphues, V. S. Yakovlev, A. Baltuška, B. Horvath, B. Schmidt, L. Blümel, R. Holzwarth, S. Hendel, M. Drescher, U. Kleineberg, P. M. Echenique, R. Kienberger, F. Krausz, and U. Heinzmann, "Attosecond spectroscopy in condensed matter," Nature 449, 1029 (2007).

[80] Y. Mairesse and F. Quéré, "Frequency-resolved optical gating for complete reconstruction of attosecond bursts," Phys. Rev. A 71, 011401 (2005).

[81] M. Chini, S. Gilbertson, S. D. Khan, and Z. Chang, "Characterizing ultrabroadband attosecond lasers," Opt. Express 18, 13006 (2010).

[82] V. Gruson, L. Barreau, Á. Jiménez-Galan, F. Risoud, J. Caillat, A. Maquet, B. Carré, F. Lepetit, J.-F. Hergott, T. Ruchon, L. Argenti, R. Taïeb, F. Martín, and P. Salières, "Attosecond dynamics through a Fano resonance: Monitoring the birth of a photoelectron," Science 354, 734 (2016).

[83] D. Busto, L. Barreau, M. Isinger, M. Turconi, C. Alexandridi, A. Harth, S. Zhong, R. J. Squibb, D. Kroon, S. Plogmaker, M. Miranda, Á. Jiménez-Galán, L. Argenti, C. L. Arnold, R. Feifel, F. Martín, M. Gisselbrecht, A. L'Huillier, and P. Salières, "Time–frequency representation of autoionization dynamics in helium," J. Phys. B: At., Mol. Opt. Phys. 51, 044002 (2018).

[84] L. A. A. Nikolopoulos, E. P. Benis, P. Tzallas, D. Charalambidis, K. Witte, and G. D. Tsakiris, "Second order autocorrelation of an XUV attosecond pulse train," Phys. Rev. Lett. 94, 113905 (2005).

[85] Y. Kobayashi, T. Ohno, T. Sekikawa, Y. Nabekawa, and S. Watanabe, "Pulse width measurement of high-order harmonics by autocorrelation," Appl. Phys. B 70, 389 (2000).

[86] N. A. Papadogiannis, L. A. A. Nikolopoulos, D. Charalambidis, G. D. Tsakiris, P. Tzallas, and K. Witte, "Two-photon ionization of He through a superposition of higher harmonics," Phys. Rev. Lett. 90, 133902 (2003).

[87] E. P. Benis, P. Tzallas, L. A. A. Nikolopoulos, M. Kovačev, C. Kalpouzos, D. Charalambidis, and G. D. Tsakiris, "Frequency-resolved photoelectron spectra of two-photon ionization of He by an attosecond pulse train," New J. Phys. 8, 92 (2006).

[88] D. Descamps, L. Roos, C. Delfin, A. L'Huillier, and C.-G. Wahlström, "Two- and three-photon ionization of rare gases using femtosecond harmonic pulses generated in a gas medium," Phys. Rev. A 64, 031404(R) (2001).

[89] N. Tsatrafyllis, I. Bergues, H. Schroder, L. Veisz, E. Skantzakis, D. Gray, B. Bodi, S. Kuhn, G. D. Tsakiris, D. Charalambidis, and P. Tzallas, "The ion microscope as a tool for quantitative measurements in the extreme ultraviolet," Sci. Rep. 6, 21556 (2016).

[90] P. Tzallas, B. Bergues, D. Rompotis, N. Tsatrafyllis, S. Chatziathanassiou, A. Muschet, L. Veisz, H. Schröder, and D. Charalambidis, "Time gated ion microscopy of light-atom interactions," J. Opt. 20, 24018 (2018).

[91] G. Kolliopoulos, B. Bergues, H. Schröder, P. A. Carpeggiani, L. Veisz, G. D. Tsakiris, D. Charalambidis, and P. Tzallas, "Revealing quantum path details in high-field physics," Phys. Rev. A 90, 013822 (2015).

[92] B. Bergues, D. E. Rivas, M. Weidman, A. A. Muschet, W. Helml, A. Guggenmos, V. Pervak, U. Kleineberg, G. Marcus, R. Kienberger, D. Charalambidis, P. Tzallas, H. Schröder, F. Krausz, and L. Veisz, "Tabletop nonlinear optics in the 100-eV spectral region," Optica 5, 237 (2018).

[93] R. Hörlein, Y. Nomura, P. Tzallas, S. G. Rykovanov, B. Dromey, J. Osterhoff, Z. Major, S. Karsch, L. Veisz, M. Zepf, D. Charalambidis, F. Krausz, and G. D. Tsakiris, "Temporal characterization of attosecond pulses emitted from solid-density plasmas," New J. Phys. 12, 043020 (2010).

[94] O. Faucher, P. Tzallas, E. P. Benis, J. Kruse, A. Peralta Conde, C. Kalpouzos, and D. Charalambidis, "Four-dimensional investigation of the 2nd order volume autocorrelation technique," Appl. Phys. B 97, 505 (2009).

[95] H. Mashiko, A. Suda, and K. Midorikawa, "All-reflective interferometric autocorrelator for the measurement of ultra-short optical pulses," Appl. Phys. B 76, 525 (2003).

[96] A. Peralta Conde, J. Kruse, O. Faucher, P. Tzallas, E. P. Benis, and D. Charalambidis, "Realization of time-resolved two-vacuum-ultraviolet-photon ionization," Phys. Rev. A 79, 061405 (2009).

[97] D. Charalambidis, P. Tzallas, E. P. Benis, and G. D. Tsakiris, "Attosecond scale multi-XUV-photon processes," in Progress in Ultrafast Intense Laser Science, Springer Series in Chemical Physics Vol. 91, edited by K. Yamanouchi, A. Becker, R. Li, and S. L. Chin (Springer, Berlin, Heidelberg, 2009).

[98] J. E. Kruse, P. Tzallas, E. Skantzakis, C. Kalpouzos, G. D. Tsakiris, and D. Charalambidis, "Inconsistencies between two attosecond pulse metrology methods: A comparative study," Phys. Rev. A 82, 021402(R) (2010).

[99] P. Tzallas, E. Skantzakis, and D. Charalambidis, "Direct two-XUV-photon double ionization in xenon," J. Phys. B: At., Mol. Opt. Phys. 45, 074007 (2012).

[100] P. Tzallas, E. Skantzakis, C. Kalpouzos, E. P. Benis, G. D. Tsakiris, and D. Charalambidis, "Generation of intense continuum extreme-ultraviolet radiation by many-cycle laser fields," Nat. Phys. 3, 846 (2007).

[101] G. Kolliopoulos, P. A. Carpeggiani, D. Rompotis, D. Charalambidis, and P. Tzallas, "A compact collinear polarization gating scheme for many cycle laser pulses," Rev. Sci. Instrum. 83, 063102 (2012).

[102] Y. Nabekawa, T. Shimizu, T. Okino, K. Furusawa, H. Hasegawa, K. Yamanouchi, and K. Midorikawa, "Interferometric autocorrelation of an attosecond pulse train in the single-cycle regime," Phys. Rev. Lett. 97, 153904 (2006).

[103] R. Trebino, Frequency-Resolved Optical Gating: The Measurement of Ultrashort Laser Pulses (Springer Science & Business Media, 2000).

[104] V. Véniard, R. Taïeb, and A. Maquet, "Phase dependence of (N+1)-color (N>1) IR-UV photoionization of atoms with higher harmonics," Phys. Rev. A 54, 721 (1996).

[105] R. López-Martens, K. Varjú, P. Johnsson, J. Mauritsson, Y. Mairesse, P. Salières, M. B. Gaarde, K. J. Schafer, A. Persson, S. Svanberg, C.-G. Wahlström, and A. L'Huillier, "Amplitude and phase control of attosecond light pulses," Phys. Rev. Lett. 94, 033001 (2005).

[106] H. G. Muller, "Reconstruction of attosecond harmonic beating by interference of two-photon transitions," Appl. Phys. B 74, s17 (2002).

[107] Y. Mairesse, A. de Bohan, L. J. Frasinski, H. Merdji, L. C. Dinu, P. Monchicourt, P. Breger, M. Kovačev, R. Taïeb, B. Carré, H. G. Muller, P. Agostini, and P. Salières, "Attosecond synchronization of high-harmonic soft x-rays," Science 302, 1540 (2003).

[108] K. Varjú, P. Johnsson, R. López-Martens, T. Remetter, E. Gustafsson, J. Mauritsson, M. B. Gaarde, K. J. Schafer, Ch. Erny, I. Sola, A. Zaïr, E. Constant, E. Cormier, E. Mével, and A. L'Huillier, "Experimental studies of attosecond pulse trains," Laser Phys. 15, 888 (2005).

[109] S. Haessler, B. Fabre, J. Higuet, J. Caillat, T. Ruchon, P. Breger, B. Carré, E. Constant, A. Maquet, E. Mével, P. Salières, R. Taïeb, and Y. Mairesse, "Phase-resolved attosecond near-threshold photoionization of molecular nitrogen," Phys. Rev. A 80, 011404 (2009).

[110] R. Locher, L. Castiglioni, M. Lucchini, M. Greif, L. Gallmann, J. Osterwalder, M. Hengsberger, and U. Keller, "Energy-dependent photoemission delays from noble metal surfaces by attosecond interferometry," Optica 2, 405 (2015).

[111] S. Heuser, A. Jiménez Galán, C. Cirelli, C. Marante, M. Sabbar, R. Boge, M. Lucchini, L. Gallmann, I. Ivanov, A. S. Kheifets, J. M. Dahlström, E. Lindroth, L. Argenti, F. Martín, and U. Keller, "Angular dependence of photoemission time delay in helium," Phys. Rev. A 94, 063409 (2016).

[112] M. Schultze, M. Fieß, N. Karpowicz, J. Gagnon, M. Korbman, M. Hofstetter, S. Neppl, A. L. Cavalieri, Y. Komninos, Th. Mercouris, C. A. Nicolaides, R. Pazourek, S. Nagele, J. Feist, J. Burgdörfer, A. M. Azzeer, R. Ernstorfer, R. Kienberger, U. Kleineberg, E. Goulielmakis, F. Krausz, and V. S. Yakovlev, "Delay in photoemission," Science 328, 1658 (2010).

[113] M. Isinger, R. J. Squibb, D. Busto, S. Zhong, A. Harth, D. Kroon, S. Nandi, C. L. Arnold, M. Miranda, J. M. Dahlström, E. Lindroth, R. Feifel, M. Gisselbrecht,

and A. L'Huillier, "Photoionization in the time and frequency domain," Science **358**, 893 (2017).

[114]J. M. Dahlström, A. L'Huillier, and A. Maquet, "Introduction to attosecond delays in photoionization," J. Phys. B: At., Mol. Opt. Phys. **45**, 183001 (2012).

[115]E. S. Toma and H. G. Muller, "Calculation of matrix elements for mixed extreme ultraviolet-infrared two-photon above-threshold ionization of argon," J. Phys. B: At., Mol. Opt. Phys. **35**, 3435 (2002).

[116]K. Varjú, Y. Mairesse, P. Agostini, P. Breger, B. Carré, L. J. Frasinski, E. Gustafsson, P. Johnsson, J. Mauritsson, H. Merdji, P. Monchicourt, A. L'Huillier, and P. Salières, "Reconstruction of attosecond pulse trains using an adiabatic phase expansion," Phys. Rev. Lett. **95**, 243901 (2005).

[117]J. Mauritsson, M. B. Gaarde, and K. J. Schafer, "Accessing properties of electron wave packets generated by attosecond pulse trains through time-dependent calculations," Phys. Rev. A **72**, 013401 (2005).

[118]K. Klünder, J. M. Dahlström, M. Gisselbrecht, T. Fordell, M. Swoboda, D. Guénot, P. Johnsson, J. Caillat, J. Mauritsson, A. Maquet, R. Taïeb, and A. L'Huillier, "Probing single-photon ionization on the attosecond time scale," Phys. Rev. Lett. **106**, 143002 (2011).

[119]C. Palatchi, J. M. Dahlström, A. S. Kheifets, I. A. Ivanov, D. M. Canaday, P. Agostini, and L. F. DiMauro, "Atomic delay in helium, neon, argon and krypton," J. Phys. B: At., Mol. Opt. Phys. **47**, 245003 (2014).

[120]E. Lindroth and J. M. Dahlström, "Attosecond delays in laser-assisted photodetachment from closed-shell negative ions," Phys. Rev. A **96**, 013420 (2017).

[121]E. Goulielmakis, M. Schultze, M. Hofstetter, V. S. Yakovlev, J. Gagnon, M. Uiberacker, A. L. Aquila, E. M. Gullikson, D. T. Attwood, R. Kienberger, F. Krausz, and U. Kleineberg, "Single-cycle nonlinear optics," Science **320**, 1614 (2008).

[122]F. Ferrari, F. Calegari, M. Lucchini, C. Vozzi, S. Stagira, G. Sansone, and M. Nisoli, "High-energy isolated attosecond pulses generated by above-saturation few-cycle fields," Nat. Photonics **4**, 875 (2010).

[123]O. Tcherbakoff, E. Mevel, D. Descamps, J. Plumridge, and E. Constant, "Time-gated high-order harmonic generation," Phys. Rev. A **68**, 043804 (2003).

[124]G. Sansone, E. Benedetti, F. Calegari, C. Vozzi, L. Avaldi, R. Flammini, L. Poletto, P. Villoresi, C. Altucci, R. Velotta, S. Stagira, S. De Silvestri, and M. Nisoli, "Isolated single-cycle attosecond pulses," Science **314**, 443 (2006).

[125]H. Mashiko, S. Gilbertson, C. Li, S. D. Khan, M. M. Shakya, E. Moon, and Z. Chang, "Double optical gating of high-order harmonic generation with carrier-envelope phase stabilized lasers," Phys. Rev. Lett. **100**, 103906 (2008).

[126]Y. Oishi, M. Kaku, A. Suda, F. Kannari, and K. Midorikawa, "Generation of extreme ultraviolet continuum radiation driven by a sub-10-fs two-color field," Opt. Express **14**, 7230 (2006).

[127]H. C. Bandulet, D. Comtois, E. Bisson, A. Fleischer, H. Pépin, J.-C. Kieffer, P. B. Corkum, and D. M. Villeneuve, "Gating attosecond pulse train generation using multicolor laser fields," Phys. Rev. A **81**, 013803 (2010).

[128]K. T. Kim, C. Zhang, T. Ruchon, J.-F. Hergott, T. Auguste, D. Villeneuve, P. Corkum, and F. Quéré, "Photonic streaking of attosecond pulse trains," Nat. Photonics **7**, 651 (2013).

[129]M. B. Gaarde and K. J. Schafer, "Generating single attosecond pulses via spatial filtering," Opt. Lett. **31**, 3188 (2006).

[130]E. Constant, V. D. Taranukhin, A. Stolow, and P. B. Corkum, "Methods for the measurement of the duration of high-harmonic pulses," Phys. Rev. A **56**, 3870 (1997).

[131]R. Kienberger, E. Goulielmakis, M. Uiberacker, A. Baltuska, V. Yakovlev, F. Bammer, A. Scrinzi, T. Westerwalbesloh, U. Kleineberg, U. Heinzmann, M. Drescher, and F. Krausz, "Atomic transient recorder," Nature **427**, 817 (2004).

[132]B. Förg, "Attosecond dynamics of collective electron effects in nanostructures and molecules," Ph.D. thesis, Ludwig-Maximilians-Universität, 2017.

[133]F. Quéré, Y. Mairesse, and J. Itatani, "Temporal characterization of attosecond XUV fields," J. Mod. Opt. **52**, 339 (2005).

[134]R. Trebino, K. W. DeLong, D. N. Fittinghoff, J. N. Sweetser, M. A. Krumbügel, B. A. Richman, and D. J. Kane, "Measuring ultrashort laser pulses in the time-frequency domain using frequency-resolved optical gating," Rev. Sci. Instrum. **68**, 3277 (1997).

[135]J. Gagnon, E. Goulielmakis, and V. S. Yakovlev, "The accurate FROG characterization of attosecond pulses from streaking measurements," Appl. Phys. B **92**, 25 (2008).

[136]I. Thomann, A. Bahabad, X. Liu, R. Trebino, M. M. Murnane, and H. C. Kapteyn, "Characterizing isolated attosecond pulses from hollow-core waveguides using multi-cycle driving pulses," Opt. Express **17**, 4611 (2009).

[137]M. Lucchini, M. H. Brügmann, A. Ludwig, L. Gallmann, U. Keller, and T. Feurer, "Ptychographic reconstruction of attosecond pulses," Opt. Express **23**, 29502 (2015).

[138]P. D. Keathley, S. Bhardwaj, J. Moses, G. Laurent, and F. X. Kärtner, "Volkov transform generalized projection algorithm for attosecond pulse characterization," New J. Phys. **18**, 073009 (2016).

[139]I. Thomann, E. Gregonis, X. Liu, R. Trebino, A. S. Sandhu, M. M. Murnane, and H. C. Kapteyn, "Temporal characterization of attosecond wave forms in the sub-optical-cycle regime," Phys. Rev. A **78**, 011806(R) (2008).

[140]K. T. Kim, D. H. Ko, J. Park, V. Tosa, and C. H. Nam, "Complete temporal reconstruction of attosecond high-harmonic pulse trains," New J. Phys. **12**, 083019 (2010).

[141]M. Kitzler, N. Milosevic, A. Scrinzi, F. Krausz, and T. Brabec, "Quantum theory of attosecond XUV pulse measurement by laser dressed photoionization," Phys. Rev. Lett. **88**, 173904 (2002).

[142]M. Lucchini, G. D. Lucarelli, M. Murari, A. Trabattoni, N. Fabris, F. Frassetto, S. De Silvestri, L. Poletto, and M. Nisoli, "Few-femtosecond extreme-ultraviolet pulses fully reconstructed by a ptychographic technique," Opt. Express **26**, 6771 (2018).

[143]K. Zhao, Q. Zhang, M. Chini, Y. Wu, X. Wang, and Z. Chang, "Tailoring a 67 attosecond pulse through advantageous phase-mismatch," Opt. Lett. **37**, 3891 (2012).

[144]G. Kolliopoulos, P. Tzallas, B. Bergues, P. A. Carpeggiani, P. Heissler, H. Schröder, L. Veisz, D. Charalambidis, and G. D. Tsakiris, "Single-shot autocorrelator for extreme-ultraviolet radiation," J. Opt. Soc. Am. B **31**, 926 (2014).

[145]E. Gustafsson, T. Ruchon, M. Swoboda, T. Remetter, E. Pourtal, R. López-Martens, Ph. Balcou, and A. L'Huillier, "Broadband attosecond pulse shaping," Opt. Lett. **32**, 1353 (2007).

[146]M. Swoboda, J. M. Dahlström, T. Ruchon, P. Johnsson, J. Mauritsson, A. L'Huillier, and K. J. Schafer, "Intensity dependence of laser-assisted attosecond photoionization spectra," Laser Phys. **19**, 1591 (2009).

[147]C. Bourassin-Bouchet and M.-E. Couprie, "Partially coherent ultrafast spectrography," Nat. Commun. **6**, 6465 (2015).

[148]M. Isinger, D. Busto, S. Mikaelsson, S. Zhong, C. Guo, P. Salières, C. L. Arnold, A. L'Huillier, and M. Gisselbrecht, "Accuracy and precision of the RABBIT technique," Philos. Trans. R. Soc., A **377**, 20170475 (2019).

[149]V. S. Yakovlev, F. Bammer, and A. Scrinzi, "Attosecond streaking measurements," J. Mod. Opt. **52**, 395 (2005).

[150]J. Gagnon and V. S. Yakovlev, "The robustness of attosecond streaking measurements," Opt. Express **17**, 17678 (2009).

[151]H. Wang, M. Chini, S. D. Khan, S. Chen, S. Gilbertson, X. Feng, H. Mashiko, and Z. Chang, "Practical issues of retrieving isolated attosecond pulses," J. Phys. B: At., Mol. Opt. Phys. **42**, 134007 (2009).

[152]A. S. Kheifets, "Time delay in valence-shell photoionization of noble-gas atoms," Phys. Rev. A **87**, 063404 (2013).

[153]S. Pabst and J. M. Dahlström, "Eliminating the dipole phase in attosecond pulse characterization using Rydberg wave packets," Phys. Rev. A **94**, 013411 (2016).

[154]J. M. Dahlström, S. Pabst, and E. Lindroth, "Pulse analysis by delayed absorption from a coherently excited atom," APL Photonics **4**, 011101 (2019).

[155]J. White and Z. Chang, "Attosecond streaking phase retrieval with neural network," Opt. Express **27**, 4799 (2019).

[156]P. Tzallas, E. Skantzakis, and D. Charalambidis, "Measuring the absolute carrier-envelope phase of many-cycle laser fields," Phys. Rev. A **82**, 061401(R) (2010).

[157]Y. Nabekawa, H. Hasegawa, E. J. Takahashi, and K. Midorikawa, "Production of doubly charged helium ions by two-photon absorption of an intense sub-10-fs soft x-ray pulse at 42 eV photon energy," Phys. Rev. Lett. **94**, 043001 (2005).

[158]N. Miyamoto, M. Kamei, D. Yoshitomi, T. Kanai, T. Sekikawa, T. Nakajima, and S. Watanabe, "Observation of two-photon above-threshold ionization of rare gases by xuv harmonic photons," Phys. Rev. Lett. **93**, 083903 (2004).

[159]P. Heissler, R. Hörlein, J. M. Mikhailova, L. Waldecker, P. Tzallas, A. Buck, K. Schmid, C. M. S. Sears, F. Krausz, L. Veisz, M. Zepf, and G. D. Tsakiris, "Few-cycle driven relativistically oscillating plasma mirrors: A source of intense isolated attosecond pulses," Phys. Rev. Lett. **108**, 235003 (2012).

[160]F. H. M. Faisal, *Theory of Multiphoton Processes* (Plenum, New York, 1987).

[161]M. A. Kornberg and P. Lambropoulos, "Photoelectron energy spectrum indirect two-photon double ionization of helium," J. Phys. B: At., Mol. Opt. Phys. **32**, L603 (1999).

[162]P. Lambropoulos, L. A. A. Nikolopoulos, and M. G. Makris, "Signatures of direct double ionization under XUV radiation," Phys. Rev. A **72**, 727 (2005).

[163]K. D. Schultz, C. I. Blaga, R. Chirla, P. Colosimo, J. Cryan, A. M. March, C. Roedig, E. Sistrunk, J. Tate, J. Wheeler, P. Agostini, and L. F. DiMauro, "Strong field physics with long wavelength lasers," J. Mod. Opt. **54**, 1075 (2007).

[164]V. S. Yakovlev, M. Ivanov, and F. Krausz, "Enhanced phase-matching for generation of soft x-ray harmonics and attosecond pulses in atomic gases," Opt. Express **15**, 15351 (2007).

[165]S. L. Cousin, F. Silva, S. Teichmann, M. Hemmer, B. Buades, and J. Biegert, "High-flux table-top soft x-ray source driven by sub-2-cycle, CEP stable, 1.85-μm 1-kHz pulses for carbon K-edge spectroscopy," Opt. Lett. **39**, 5383 (2014).

[166]S. L. Cousin, N. Di Palo, B. Buades, S. M. Teichmann, M. Reduzzi, M. Devetta, A. Kheifets, G. Sansone, and J. Biegert, "Attosecond streaking in the water window: A new regime of attosecond pulse characterization," Phys. Rev. X **7**, 041030 (2017).

[167]X. Ren, J. Li, Y. Yin, K. Zhao, A. Chew, Y. Wang, S. Hu, Y. Cheng, E. Cunningham, Y. Wu, M. Chini, and Z. Chang, "Attosecond light sources in the water window," J. Opt. **20**, 023001 (2018).

[168]R. Budriūnas, T. Stanislauskas, J. Adamonis, A. Aleknavičius, G. Veitas, D. Gadonas, S. Balickas, A. Michailovas, and A. Varanavičius, "53 W average power CEP-stabilized OPCPA system delivering 5.5 TW few cycle pulses at 1 kHz repetition rate," Opt. Express **25**, 5797 (2017), https://www.eli-alps.hu/en/Research-Technology/Lasers.

[169]In the present article, we have tried to include all representative papers in the field of attosecond pulse metrology. Given the existence of a vast number of relevant literature in the field, we apologize for any unintentional omission of original research papers having significant contribution on the development of the field.